frontiers | Frontiers in Geochemistry

TYPE Hypothesis and Theory
PUBLISHED 25 March 2024
DOI 10.3389/fgeoc.2024.1366268

OPEN ACCESS

EDITED BY
Florian Osselin,
UMR7327 Institut des Sciences de la Terre d'Orléans (ISTO), France

REVIEWED BY
Eric C. Gaucher,
Lavoisier H2 Geoconsult, France
Laurent Truche,
Université Grenoble Alpes, France
Marguerite Godard,
UMR5243 Géosciences Montpellier, France

*CORRESPONDENCE
Alexis S. Templeton,
alexis.templeton@colorado.edu

RECEIVED 05 January 2024
ACCEPTED 04 March 2024
PUBLISHED 25 March 2024

CITATION
Templeton AS, Ellison ET, Kelemen PB, Leong J, Boyd ES, Colman DR and Matter JM (2024), Low-temperature hydrogen production and consumption in partially-hydrated peridotites in Oman: implications for stimulated geological hydrogen production.
Front. Geochem. 2:1366268.
doi: 10.3389/fgeoc.2024.1366268

Low-temperature hydrogen production and consumption in partially-hydrated peridotites in Oman: implications for stimulated geological hydrogen production

Alexis S. Templeton[1]*, Eric T. Ellison[1], Peter B. Kelemen[2], James Leong[2], Eric S. Boyd[3], Daniel R. Colman[3] and Juerg M. Matter[4]

[1]Department of Geological Sciences, University of Colorado, Boulder, CO, United States, [2]Department of Lamont Doherty Earth Observatory, Columbia University, New York, NY, United States, [3]Department of Microbiology and Cell Biology, Montana State University, Bozeman, MT, United States, [4]School of Ocean and Earth Science, University of Southampton, Southampton, United Kingdom

The Samail Ophiolite in Oman, the largest exposed body of ultramafic rocks at the Earth's surface, produces a continuous flux of hydrogen through low-temperature water/rock reactions. In turn, the scale of the subsurface microbial biosphere is sufficient to consume much of this hydrogen, except where H_2 is delivered to surface seeps via faults. By integrating data from recent investigations into the alteration history of the peridotites, groundwater dynamics, and the serpentinite-hosted microbial communities, we identify feasible subsurface conditions for a pilot demonstration of stimulated geological hydrogen production. A simple technoeconomic analysis shows that the stimulation methods to be used must increase the rate of net hydrogen production at least 10,000-fold compared to the estimated natural rate to economically produce hydrogen from engineered water/rock reactions in the peridotite formations. It may be possible to meet this challenge within the upper 1–2 km, given the projected availability of reactive Fe(II)-bearing phases and the lower drilling costs associated with shallower operations. Achieving ≥10,000-fold increases in the H_2 production rate will require a combination of stimuli. It will likely be necessary to increase the density of fracturing in the reaction volume by at least two orders of magnitude. Then, the H_2-production rates must also be increased by another two orders of magnitude by increasing the water/rock ratio and modifying the chemistry of the injected fluids to optimize formation of Fe(III)-bearing secondary phases. These fluid modifications must be designed to simultaneously minimize microbial consumption of H_2 within the stimulation volume. In contrast, preserving the high potentials for biological H_2 consumption in the shallow groundwaters replete with oxidants such as nitrate, sulfate and dissolved inorganic carbon will reduce the potential for any inadvertent leaks of hydrogen to the atmosphere, where it acts as an indirect greenhouse gas.

KEYWORDS

peridotite, hydrogen, serpentinization, microbial, stimulation

1 Introduction

Hydrogen has powered living microbial ecosystems on Earth for billions of years (McCollom and Shock, 1997; Sleep et al., 2004; Hellevang et al., 2011; Martin, 2012; Colman et al., 2017; Boyd et al., 2020; Templeton and Caro, 2023). Today hydrogen is of intense interest as a versatile, low-carbon energy carrier sought in the chemical, transportation and energy sectors globally. Combustion of hydrogen is attractive in energy generation because it does not directly produce emissions of CO_2 or other pollutants (Gaucher et al., 2023). Major policy and investment initiatives to build critical infrastructure required for hydrogen pipelines, conversion and storage are occurring globally, coupled with efforts to develop sufficient sources of hydrogen that can meet global demand and support reaching net-zero by 2050. However, several of the current or planned sources of hydrogen will exert a notable environmental footprint and create large raw material demands to create and separate the hydrogen, including "low-carbon hydrogen" such as steam methane reforming and electrolysis.

Fortunately, low-carbon hydrogen is also produced through natural geological processes, although the locations and amounts of geological hydrogen currently stored in the Earth's subsurface are poorly constrained. Current exploration is focused on terrains surrounding mafic and ultramafic rock massifs previously emplaced on land or exhumed along tectonic plate boundaries, where H_2-producing serpentinization reactions have prevailed (Neal and Stanger, 1983; Sano et al., 1985; Coveney et al., 1987; Abrajano et al., 1990; Hosgormez et al., 2008; Manatschal and Müntener, 2009; Vacquand, 2011; Morrill et al., 2013; Deville and Prinzhofer, 2016; Etiope et al., 2017; Lefeuvre et al., 2021; Pasquet et al., 2021; Combaudon et al., 2022, as just a few examples). Hydrogen exploration also extends to Precambrian cratons where H_2 has accumulated through long-term radiolysis reactions (Sherwood Lollar et al., 1993, 1997; Truche et al., 2018; Warr et al., 2019, as just a few examples) or through the oxidation of Fe(II)-bearing phases in ancient sedimentary rocks such as Banded Iron formations (Moretti et al., 2022; Geymond et al., 2023). It is likely that more than 1 Mt H_2 is produced through water/rock reactions on Earth each year (see varying estimates from Sherwood Lollar et al., 2014; Klein et al., 2020; Meredith et al., 2020; Zgonnik, 2020), giving rise to intense interest in finding reservoirs that may store a fraction of this hydrogen flux, and drilling into them to obtain natural hydrogen.

The concept of "stimulated geological hydrogen" production is gaining traction as another way in which hydrogen could be produced on a large scale with a low-carbon footprint, wherever the appropriate geological conditions exist. "Stimulated geological hydrogen" is an engineering concept, whereby fluids could be injected into target rock formations rich in reactive Fe(II)-bearing minerals to promote the overarching reaction of $2FeO_{(rock)} + H_2O \rightarrow Fe_2O_{3(rock)} + H_2$. Then H_2 is extracted by recirculating those fluids to the surface, if the required (bio) geochemical conditions for rapid hydrogen production have been met. Recently published, optimistic estimates of "stimulated hydrogen production" (also originally termed "orange hydrogen") suggest that up to 100 trillion tonnes of H_2 could be produced from Fe(II)-bearing rocks near Earth's surface (Osselin et al., 2022). Given the potential impact of this solution, the U.S. Department of Energy recently allocated funding to investigate stimulated H_2 production using various stimuli, as well as characterization of the properties of target source rocks and reservoirs.

Numerous potential Fe(II)-bearing source rocks may yield some hydrogen during water/rock reaction, although many protoliths have not yet been carefully tested. Equilibrium thermodynamic models can be used to predict potential hydrogen yields. The best targets for stimulated hydrogen production are rocks such as peridotites, which can produce 2–4 kg hydrogen/m^3 of rock, up to 4-orders of magnitude more hydrogen than mafic rocks such as basalts (Bach, 2016; Leong et al., 2021a; Osselin et al., 2022; Ely et al., 2023). For serpentinization of ultramafic rocks, the integrated set of reactions that couple the oxidation of mineral-derived Fe(II) to the reduction of water to produce hydrogen gas are predicted to occur at maximum extents at temperatures between 200 and 300°C (McCollom and Bach, 2009; Klein et al., 2013). However, reaching these high temperatures in an engineered system requires either initiating water/rock reactions at great depth, or adjacent to hydrothermally-active geological systems, or in rocks heated by large inputs of energy.

However, it is notable that hydrogen naturally occurs in seeps and groundwaters in shallow ultramafic rock formations, leading to the possibility that some hydrogen producing reactions do proceed at temperatures ≤100°C. This hydrogen flux may be sustained through active water/rock reactions, or may be derived from fossil hydrogen produced at depth and stored within the peridotite. Locations on Earth where abundant hydrogen has been measured in seeps and groundwaters emanating from ultramafic rocks include the Philippines (Abrajano et al., 1988, 1990; Cardace et al., 2015; Vacquand et al., 2018), Turkey (Hosgormez et al., 2008; Etiope et al., 2011; Vacquand et al., 2018); Italy (Boschetti et al., 2013); New Caledonia (Monnin et al., 2014, 2021; Deville and Prinzhofer, 2016; Vacquand et al., 2018), California (Cardace et al., 2013; Morrill et al., 2013; Suzuki et al., 2013; Cook et al., 2021), Canada (Szponar et al., 2013), as well as Oman (Neal and Stanger, 1983; Boulart et al., 2013; Vacquand et al., 2018; Zgonnik et al., 2019; Leong et al., 2023). To solve the enigma of why H_2 is so prevalent under conditions where we expect slow reaction rates and yields, more of the reactions governing H_2 production need to be investigated under the conditions of temperature, fluid chemistry, pH and protolith buffering in low-temperature ophiolite systems.

It is also critical to start assessing the feasibility of engineering subsurface stimulated H_2-producing water/rock reactions through *in-situ* experimentation. The challenge is to promote the optimal hydrogeochemical conditions that give rise to the fastest H_2 production and the highest yield of H_2 produced per volume of rock. Initial H_2 production will depend on many factors, such as the temperature of the rocks, the water/rock ratio, the chemical composition of the fluids and rocks, and the initial fracture network required for fluid injection. Continued H_2 production will be dependent upon how the permeability, mineralogy and Fe-oxidation state of the rocks evolves, as well as the extent of *in-situ* biological H_2 production and consumption.

This work provides a specific hypothesis and supporting theory for why the Sultanate of Oman might be one of the best geological locations to engineer stimulated subsurface H_2 production in peridotite rocks. Although anywhere from 40 to >90% of the total Fe in the target peridotite formations has already been

oxidized through prior water/rock reaction (Mayhew et al., 2018; Ellison et al., 2021), H_2 is continually being produced by modern water/rock reactions with low salinity fluids under long-residence time, low-temperature conditions (≤50°C) (Miller et al., 2017; Ellison et al., 2021; Kelemen et al., 2021). From spectroscopic analysis of reaction sequences preserved in partially-altered Oman rocks, it can be inferred that geological hydrogen is produced through reactions involving the oxidation of Fe(II) in primary silicates (e.g., olivine and pyroxene) and secondary phases (e.g., brucite, magnetite and Fe(II)-serpentine) to ferric phases such as magnetite, Fe(III)-serpentine, and andradite garnet (Mayhew et al., 2018; Ellison et al., 2021). Thus, there are several reactions that govern net H_2 production that could be optimized.

A key question is whether fractured, partially serpentinized peridotites can react fast enough with circulating water to produce economic quantities of hydrogen in an engineered subsurface reservoir. To make reasonable predictions, it is important to first understand the baseline state of the natural system. To date, it has been challenging to estimate the current net rates of hydrogen production in the peridotite rocks in Oman, prior to any stimulation, due to slow serpentinization and H_2 degassing rates, coupled with uncertainties about the extent of H_2 consumption by H_2-metabolizing microorganisms. Little hydrogen is detectable in soils established above the peridotite rocks (Zgonnik et al., 2019; Leong et al., 2023), perhaps due to slow production, and/or to intense microbially-catalyzed H_2 oxidation in shallow aquifers. Subsurface microbial communities have been detected in the peridotite rocks and fluids, and they exhibit highly variable rates of activity across geochemical gradients (Fones et al., 2019, 2022; Glombitza et al., 2021; Kraus et al., 2021; Templeton et al., 2021). Therefore, to begin to assess the feasibility of stimulated hydrogen production in Oman, we must first integrate our understanding of the geological, hydrological and biological controls on H_2 availability in groundwaters during active low-temperature serpentinization in the Samail ophiolite. We apply this knowledge to hypothesize how H_2 production could be stimulated through changes in the physical, chemical and biological properties of the subsurface aquifers, while also exploring some of the economic challenges that will likely be encountered.

2 Hydrogen production and consumption in Oman peridotite aquifers

2.1 H_2-producing reactions predicted during low-temperature peridotite hydration from geochemical modelling

Serpentinization processes occur through the infiltration of fluids far-from-equilibrium with Fe-rich peridotite rocks, giving rise to coupled mineral dissolution, Fe-oxidation and secondary mineralization reactions that can produce variable amounts of H_2. The recent work of Leong et al. (2021a) examines compositional controls on H_2 production during aqueous alteration of ~9,400 mafic and ultramafic rock compositions during low-temperature (25°C) aqueous alteration. Ultramafic lithologies (i.e., those with higher MgO content) have potential to generate several orders of magnitude more H_2 relative to their mafic counterparts (Figure 1A). Alteration of mafic rocks, which are more enriched in Si and Al and less enriched in Mg than ultramafic rocks, favors the formation of chlorite $[(MgFe(II))_5Al(Si_3Al)O_{10}(OH)_8]$ and clay minerals that accommodate ferrous iron into their crystal structures. When ferrous iron is transferred from the protolith into these secondary minerals, there is little Fe-oxidation, which limits H_2 generation. In contrast, the alteration of Mg-rich ultramafic rocks favors the formation of minerals enriched in ferric iron including serpentine $[(MgFe(II)Fe(III))_3\ (Fe(III)Si)_2O_5(OH)_4]$, magnetite $[Fe(III)_2Fe(II)O_4]$ and andraditic garnets $[Ca_3(Fe(III)Al)_2Si_3O_{12}]$ (e.g., Frost and Beard, 2007; McCollom and Bach, 2009; Plümper et al., 2014; Tutolo et al., 2020; Leong et al., 2021a), thereby yielding high levels of H_2.

Interestingly, in ultramafic rocks, the potential to generate H_2 will decrease as the MgO content increases from 40 to 50 wt% (Figure 1A). Rocks that are most enriched in Mg (e.g., dunite) favor formation of brucite $[(MgFe(II))(OH)_2]$. Brucite can accommodate significant amounts of ferrous iron, which then limits the extent of iron oxidation and H_2 production. Because the formation of Fe-rich brucite is also increasingly favored at low-temperatures, H_2 generation can become severely limited (McCollom and Bach, 2009). However, Fe-rich brucite can be later oxidized and remineralized as magnetite or ferric serpentine, thereby producing H_2 at later stages of water/rock reaction (Templeton and Ellison, 2020). Therefore, understanding the controls on brucite formation and loss are critically important to assessing the H_2 generating potential of low-temperature peridotite systems.

Another critical factor that controls H_2 generation is the water-rock ratio, which is the mass of water a given mass of rock had reacted with (Klein et al., 2009, 2013; McCollom and Bach, 2009; Ely et al., 2023). Brucite $[(Mg,Fe)(OH)_2]$ and serpentine with higher Fe(II)-greenalite component are favored to form at low water-rock ratios, which buffers the fluids to lower silica and higher calcium activities, respectively (Klein and Bach, 2009; Klein et al., 2009; McCollom and Bach, 2009; Frost et al., 2013; Leong and Shock, 2020; Tutolo et al., 2020; Ely et al., 2023). The overall $Fe(III)/Fe_{Total}$ of secondary phases precipitated at these conditions is low, and thus less H_2 is generated per mass of rock reacted relative to mineral assemblages formed at higher water-rock ratios (Figure 1B).

Calculations described in Figure 1B are modeled at a minimum water-rock ratio of 0.2, where the reacting fluid is fully consumed via mineral hydration reactions. The hydration of 5 kg of harzburgitic rocks into brucite-bearing serpentinites typically consumes a kg of water. Consequences of reactions at water-rock ratios lower than 0.2 will yield unreacted rocks. Thus, the H_2 generation potential of rocks with 1% porosity (i.e., water-rock ratio of 0.01) will likely yield 20-fold less H_2 than that shown for water-rock ratios of 0.2 in Figure 1B. As a given mass of rock is continuously reacted with percolating groundwater, the integrated water/rock ratio increases and the reacting rock is oxidized further. The formation of ferric-iron bearing phases such as magnetite and serpentine with higher ferric iron components (cronstedtite and/or hisingerite) is favored at higher water-rock ratios. This paragenesis is consistent with natural observations where magnetite and high $Fe(III)/Fe_{Total}$ serpentine are commonly associated with later generations of veins and highly

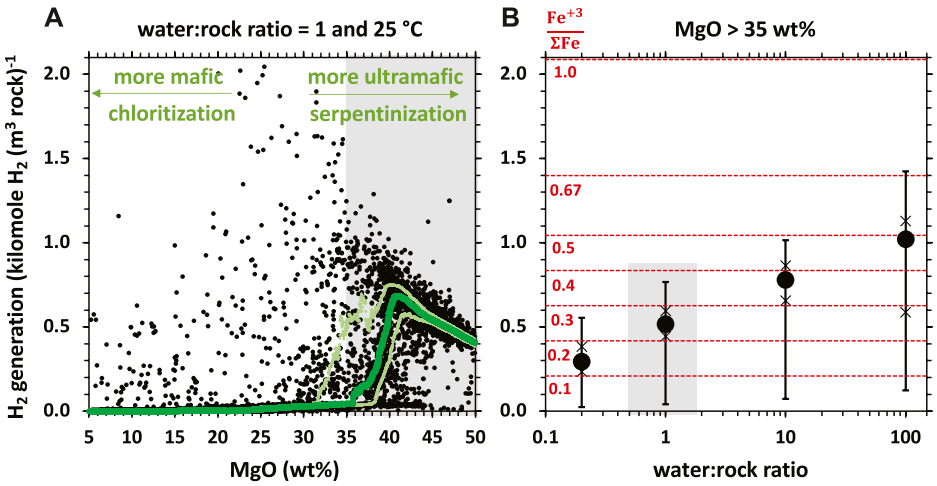

FIGURE 1
Equilibrium thermodynamic predictions of H_2 generation potential (in kilomole H_2 per m^3 of rock) of ~9,400 rocks with compositions ranging from ultramafic (higher MgO contents, towards the right side) to mafic (lower MgO contents, towards the left side), modified from Leong et al. (2021a). The green curve depicts the running median. Upper and lower light green curves are running 25th and 75th percentiles, respectively. Calculations simulate the ambient aquifer conditions in continental aquifers (25°C, 1 bar) and a low (rock-dominated) water-rock ratio of 1. **(B)** Statistical summary of thermodynamically-predicted H_2 generation potential (in kilomole H_2 per m^3 of rock) of a subset of the ~9,400 rocks in **(A)**, those with MgO content >35 wt%, at different water-rock ratios. The circle represents the median H_2 generation potential. The 25th/75th and 5th/95th percentiles are represented by the cross and horizontal tick marks, respectively. The grey highlight in **(B)** depict statistical summary at water-rock ratio of 1 for rocks with MgO >35 wt%, which is also depicted by the grey highlight in **(A)**. Dashed red lines in **(B)** depict Fe(III)/Fe_{Total} of precipitated secondary phases.

reacted or altered samples (Andreani et al., 2013b; Frost et al., 2013; Mayhew et al., 2018; Mayhew and Ellison, 2020). As shown in Figure 1B, H_2 production is maximized at a water-rock ratio of ~100, when the Fe(III)/Fe_{Total} of the bulk secondary assemblages is ~0.5 and approaches that of magnetite. At water-rock ratios greater than 100, ferric iron-bearing minerals can precipitate but H_2 production may be limited. For instance, at a very high water-rock ratio of 1,000 (i.e., each kg of aquifer host rock had reacted with 1,000 kg of water), a significant proportion of iron in the given mass of reacting rock will be oxidized by dissolved oxygen, if present in the infiltrating groundwater (~0.3 mmole O_2 per kg of air-saturated water), and will not yield H_2. Calculation results shown in Figure 1 are from batch models that can provide first-order approximation of hydrogen generation potentials of rocks of a wide range of rock compositions. Open system reactive transport experiments (e.g., Godard et al., 2013; Peuble et al., 2015; Escario et al., 2018; Oyanagi et al., 2020; Osselin et al., 2022) and models (Steefel et al., 2005; Oyanagi et al., 2020) can further offer further constraints when information such as formation porosity and permeability and mineralogical/compositional heterogeneities are available.

2.2 What H_2-producing reactions can be inferred through mineralogical analysis of Oman rocks?

Despite being 50 to >90% serpentinized, peridotites in Oman generally contain less than 0.5 wt% magnetite (Bonnemains et al., 2016; Ellison et al., 2021; Hong et al., 2022). This contrasts with many abyssal serpentinites and some ophiolites, where 1–7 wt% magnetite is commonly observed (Toft et al., 1990; Oufi et al., 2002; Klein et al., 2014). What magnetite does exist in Oman serpentinite is often found in mesh veins suggesting that it was associated with the earliest stages of serpentinization (potentially at high temperature >200°C). Additionally, increased magnetite abundance in the shallowest regions of the aquifer suggests that new magnetite is produced during later stages of weathering (Miller et al., 2016; Ellison et al., 2021; Hong et al., 2022).

The extent of rock hydration, oxidation and serpentinization in the Samail ophiolite has been characterized in detail through the recent work of the Oman Drilling Project (Kelemen et al., 2020), as summarized in Kelemen et al. (2021). Notably, the analysis of drill cores and downhole logging shows that the harzburgite and dunite rocks are fully serpentinized in the upper 100–250 m, whereas partially serpentinized rocks are present at greater depth (e.g., up to the 400 m maximum depth of the boreholes). Much of the subsurface peridotite has reacted to a serpentine-brucite assemblage (Miller et al., 2016; Ellison et al., 2021; Kelemen et al., 2021; Templeton et al., 2021). The lack of magnetite and preferential substitution of Fe into brucite, with up to 20% FeO component (Mayhew et al., 2018), is consistent with serpentinization below 200°C (e.g., Klein et al., 2014). The serpentine is a major host of both Fe(II) and Fe(III), with typically 6%–8% FeO and highly variable Fe(III)/Fe_{total} from 0.4 to 1.0, as illustrated by the example in Figure 2 (Miller et al., 2016; Mayhew et al., 2018; Ellison et al., 2021; Kelemen et al., 2021; Templeton et al., 2021). The Fe(II) that remains sequestered in brucite and in serpentine retains its potential for future H_2 production (Templeton and Ellison, 2020), in addition to Fe(II) in relict olivine (9 wt% FeO) and orthopyroxene (6 wt% FeO) (Monnier et al., 2006; Hanghøj et al., 2010).

Brucite comprises up to 8 wt% in some of the Oman Drilling Project cores (Templeton et al., 2021) or even more (≤16 wt% in some dunites), despite SiO_2 addition to peridotites during alteration

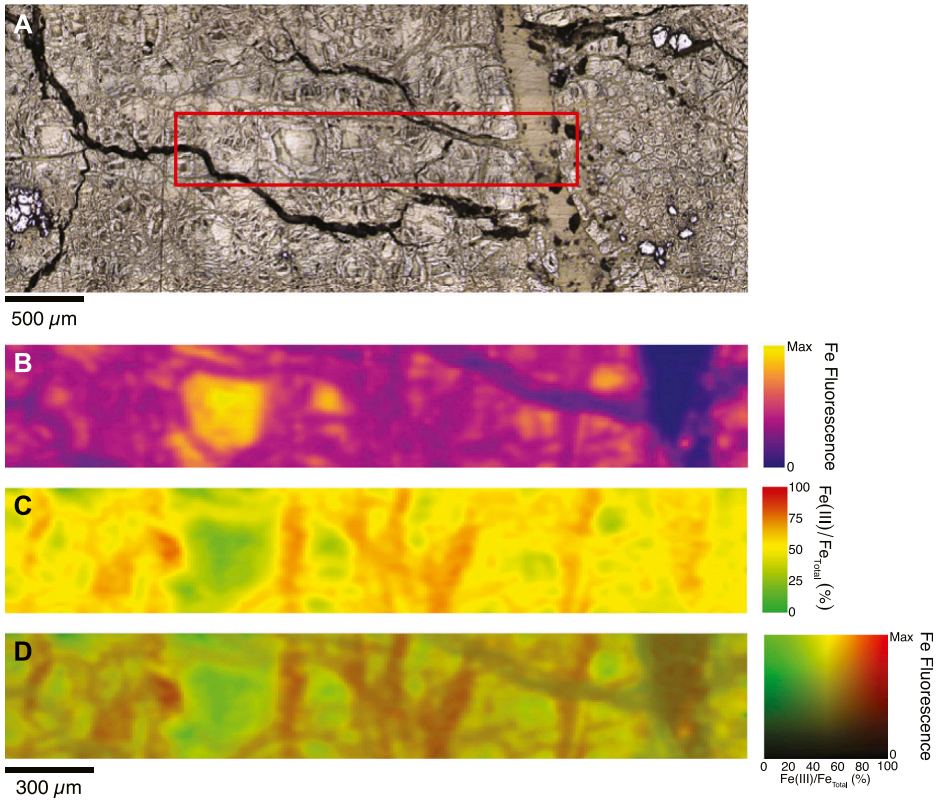

FIGURE 2
Variations in iron concentration and valence state in serpentine and brucite in a serpentinized dunite rock from the Oman subsurface, mapped using synchrotron-based X-ray Fluorescence imaging. Sample is from 110 m depth in Oman Drilling Project hole BA1B. Optical images **(A)** is used to correlate to maps of iron fluorescence **(B)**, which is proportional to the iron concentration. Variations in the Fe K-edge pre-edge feature are used to map the Fe(III)/Fe_{Total} ratio **(C)**. The information in **(B,C)** are combined to produce the image in **(D)** that shows the distribution of Fe(II) (green) and Fe(III) (red). Maps were collected using the method detailed in Ellison et al. (2021).

(Kelemen et al., 2021). Reactions that consume brucite and liberate stored Fe(II), allowing it to participate in further reactions including H_2 production, include dissolution, silicification, and carbonation (Bach et al., 2006; Tutolo et al., 2018; Ellison et al., 2021; Kelemen et al., 2021). As discussed intensively by Templeton and Ellison (2020), silicification of brucite is the replacement of brucite with serpentine or other hydrous phyllosilicates (e.g., talc). In this process, Fe may become oxidized by reaction with water, forming H_2 and a more oxidized, Fe(III)-bearing mineral product. The addition of silica to brucite forming serpentine would involve a substantial volume increase (e.g., 40%–50%), that would have to be accommodated, likely by fracturing or mass transfer. A source of excess silica would be required to drive such a reaction. This silica could be derived from serpentinization of pyroxenes, carbonation of serpentinite, or mass transfer from nearby silica-rich rocks (e.g., gabbro veins and dikes).

Hydroandradite is a garnet mineral that is common in small amounts in serpentinites (e.g., Frost and Beard, 2007; Plümper et al., 2014), including the Oman Drilling Project altered peridotite cores (Kelemen et al., 2020; Ellison et al., 2021; Kelemen et al., 2021; Templeton et al., 2021). It is a Ca^{2+}-Fe^{3+} garnet with variable amounts of OH^- substitution for SiO_4^{4-}. The Ca^{2+} is likely derived from primary clinopyroxene in peridotite. Hydroandradite is intriguing because it is expected to form only at low temperature (<230°C), highly reducing conditions, and low silica activity (e.g., Frost and Beard, 2007). Hydroandradite contains appreciable Fe^{3+} per formula unit, meaning that its precipitation could be coupled to H_2 production.

Finally, because serpentine is present in such high abundance, the amount of Fe(II) in serpentine is significant as a potential H_2 source in future water/rock reactions. For example, if the average serpentinized harzburgite in Oman contains 90 wt% serpentine, which has 95% Mg/(Mg+Fe) and 50% Fe(III)/Fe_{Total}, approximately 2 wt% of Fe(II) as FeO would then be stored by serpentine. This is almost 50% of the available reactive Fe(II) in target protoliths. The rates of oxidation of ferrous serpentine to ferric serpentine, and its coupling to H_2 production, has not yet been investigated, but there is clear evidence that fully serpentinized rocks in the Samail ophiolite are dominated by Fe(III)-bearing serpentine.

2.3 What is the current hydrological/hydrogeochemical state of Oman peridotite aquifers?

Although the partially-hydrated peridotites exhibit a low hydraulic conductivity (Dewandel et al., 2005; Lods et al., 2020), the rocks do store and transmit water and thus function as aquifers.

The rocks are fractured from the 10s of micron scale to the 10s of meters scale (Dewandel et al., 2005; Kelemen et al., 2020). Some of this fracturing is from mid-ocean ridge processes, then obduction, and most recently from surface weathering. Fluid flow occurs in the most shallow and fissured rocks in transmissive zones located within 50 m of the surface (Dewandel et al., 2005). Lods et al. (2020) found that the hydrology in two Oman Drilling Project boreholes (BA1A, BA1D) is highly heterogeneous, with some zones most sensitive to conductive channels such as a partially mineralized fractures, whereas other zones are supplied from rocks above and below. Analysis of the response of water levels in boreholes to solid Earth, ocean and atmospheric tides reveals unconfined and semi-confined aquifer conditions on short distances, confirming complex networks of crosscutting fractures partially filled with secondary minerals produced from both modern and Cretaceous water/rock reactions (Sohn and Matter, 2023). The permeabilities have been reported as 10^{-12} m^2 in the upper 50 m, to 10^{-14} m^2 up to 150 m depth and they are estimated to be extremely low (essentially not measurable, $<10^{-17}$ m^2) at greater depth in the less fractured and altered peridotite (Lods et al., 2020). This lack of permeability significantly restricts fluid circulation and the predicted extent of water/rock reaction occurring at greater depths.

In ophiolite systems, including the boreholes drilled into peridotite in the Oman Drilling Project, there are often three types of groundwaters that can be detected. The most common is known as an alkaline Type-I Mg-HCO_3^- water that forms during initial water/rock reaction in shallow fluids that exhibit short residence times and remain open to the atmosphere (Barnes and O'Neil, 1969; Paukert et al., 2012; Boulart et al., 2013; Chavagnac et al., 2013; Canovas et al., 2017; Vankeuren et al., 2019). These fluids typically contain millimolar concentrations of dissolved inorganic carbon, as well as strong oxidants such as nitrate (Rempfert et al., 2023). The measured Eh values of the fluids averages around +150 mV at pH 8.

In contrast, hyperalkaline Type II Ca-OH waters form during extensive water/rock reaction over longer residence times, sometimes even reaching chrysotile-brucite-calcite+/-diopside+/-andradite equilibrium and pH varying between pH 10 to pH 12 (as modeled in Leong and Shock, 2020; Kelemen et al., 2021; Leong et al., 2021b). In such fluids, the only dissolved oxidant present tends to be aqueous sulfate; dissolved inorganic carbon is below detection limit, and ammonium is much more abundant than nitrate (Nothaft et al., 2021b; Rempfert et al., 2023). These fluids tend to exhibit strongly reducing potentials varying from −250 to −750 mV.

The third fluid type are fluids that are mixtures of Type II fluid mixing with Type I fluids in the more shallow and fractured part of the aquifers. Although the pH is often hyperalkaline, the measured redox potentials are highly variable. The extent of mixing can often be traced by careful analysis of the dissolved silica concentrations, where ΣSi(aq) varies from 10^{-4} M in Type I fluids to 10^{-8} M in endmember Type II fluids (Leong and Shock, 2020; Leong et al., 2021b; Rempfert et al., 2023).

2.4 What hydrogen has been measured in peridotite outcrops, wells and seeps?

Diffuse outgassing in outcrops and soils may comprise a significant component of H_2 and CH_4 outgassed in ultramafic bodies, in addition to bubbling springs and gas seeps. By measuring rate of accumulation of H_2 in cm to meter scale drillholes in altered peridotite outcrops in Oman, Zgonnik et al. (2019) estimated daily H_2 outgassing that ranges from 3,200 to 6,500 moles per km^2. It is unknown if this estimate can be scaled up to the ~5,000 km^2 of exposed peridotites in Oman. In their efforts, Leong et al. (2023) did not detect H_2 or CH_4 accumulation in short-term flux experiments conducted in soils and outcrops, including those surrounding bubbling springs, and surrounding Oman Drilling Project "active-alteration" boreholes. Longer accumulation experiments or use of instruments with higher sensitivities will be necessary in future work to quantify the extent of diffuse outgassing, and to determine whether it is episodic in nature (e.g., Moretti et al., 2021). Such data will provide needed information on the transport of H_2 in the subsurface reservoir, the efficiency of biological H_2 consumption processes, and the existence of geological structures that may prevent diffuse leakage of H_2.

Dissolved H_2 has been measured in several existing groundwater monitoring wells drilled to 300 m depth in the Wadi Tayin block of the Samail Ophiolite (Miller et al., 2016; Rempfert et al., 2017; Nothaft et al., 2021b). Hydrogen is below a 10 nanomolar detection limit in fluids pumped from wells in gabbro and in peridotite wells that only intersect Type I Mg-HCO_3^- type waters, whereas dissolved H_2 concentrations as high as 2.9 millimolar have been measured in peridotite wells that intersect Type II fluids (Rempfert et al., 2017). Methane co-occurs with hydrogen in the hyperalkaline fluids, and is also present up to 1.4 millimolar in concentration (Miller et al., 2016; Rempfert et al., 2017; Nothaft et al., 2021b). These fluids also contain small molecular weight organic compounds such as formate, acetate, butyrate and propionate, but only at a few micromolar concentration (Rempfert et al., 2017; Nothaft et al., 2021b). The dissolved gas concentrations are likely underestimates, because they were not collected using gas-tight sampling techniques, and instead were brought to the surface using a submersible pump and collected using the bubble-stripping method (Nothaft, 2020), or by using a discrete 1L sampler and injecting fluid into N_2-purged vials prior to analysis of the exsolved gases by gas chromatography.

Extremely strong gradients in redox potential, which are observed as sharp decreases of up to 800 mV in Eh (or >50 orders of magnitude in fO_2) as a function of depth, have been measured in several Oman Drilling Project "active alteration" boreholes (Nothaft et al., 2021a; Ellison et al., 2021; Kelemen et al., 2021; Templeton et al., 2021). The most reducing fluids are hyperalkaline, with pH from 10–11.5, and saltier, with electrical conductivities from 2,000 to 3,350 μS/cm. Limited sampling at 275 m depth with a discrete gas-tight sampler has shown that these fluids contain high concentrations of dissolved H_2 [~1.5 mM $H_{2(aq)}$] but are not saturated with H_2 (Hoehler, Templeton, Matter et al., unpublished data).

2.5 H_2-dependent microbial communities

Geological H_2 supports the growth and activity of "lithotrophic" H_2 consuming microorganisms in mafic and ultramafic aquifers (Nealson et al., 2005; Templeton and Caro, 2023; Boyd et al., 2023 this issue). As H_2 is produced through water/rock reactions and is redistributed through advective or diffusive processes, its oxidation can be coupled to numerous microbial metabolisms that are largely dependent on the availability of electron acceptors. Such metabolisms include H_2 oxidation coupled to reduction of oxygen, nitrate, sulfate, thiosulfate, and CO_2, giving rise to metabolic products such as water (during O_2 reduction by "knallgas" bacteria), N_2 or ammonium (denitrifiers), sulfide (sulfate reducers), acetate (acetogens) and methane (methanogens), as a few examples (Vignais and Billoud, 2007; Schrenk et al., 2013; Peters et al., 2015; Greening et al., 2016, Sabuda et al., 2021). It should also be thermodynamically favorable for organisms to drive the reduction of ferric iron-bearing phases, such as hematite, goethite, ferric serpentine or magnetite, when H_2 fluxes are high. However, such Fe(III)-reducing metabolisms have not been directly studied in serpentinizing systems to date. Hydrogenotrophic Fe(III) reduction has historically been considered a process associated with (hyper)thermophiles or acidophiles, although several recent reports of H_2 oxidation coupled to Fe(III) reduction in organisms grown at circumneutral pH and low temperature (Dunham et al., 2021; Kato and Ohkuma, 2021) provide additional motivation to examine this mode of metabolism in serpentinizing systems.

In the Samail ophiolite in Oman, microbial cells are abundant in the groundwaters and partially-hydrated peridotite rocks, typically exceeding 10^5 cells/cm^3 (Fones et al., 2019; Templeton et al., 2021). Within these communities, numerous H_2-consuming organisms are regularly detected using genomic approaches applied to DNA or RNA extracted from filtered biomass. *Methanobacterium* sp., which utilize H_2/CO_2 or formate as methanogenesis substrates to produce CH_4, are some of the most commonly detected microorganisms, comprising up to 25% of the total community detected in some samples through DNA sequencing (Miller et al., 2016; Rempfert et al., 2017; Nothaft et al., 2021b; Fones et al., 2021; Kraus et al., 2021; Thieringer et al., 2023). A significant amount of the methane detected in the groundwater fluids from the Samail ophiolite is attributed to methanogenesis using H_2/CO_2 or formate based on a combination of gas chemistry, $\delta^{13}C$ CH_4 isotope, and $^{13}CH_3D$ and $^{12}CH_2D_2$ clumped isotopologue data (Nothaft et al., 2021b). These inferences are corroborated by direct measurements of biological ^{14}C-HCO_3^- reduction to CH_4 activity measurements and transcriptomic data (Fones et al., 2019; Kraus et al., 2021). Intriguingly, *Methanobacterium* populations detected in the Samail ophiolite parse into distinct lineages in the more oxidizing and CO_2 containing Type I vs. the more H_2-rich, CO_2 limited Type II fluids (Fones et al., 2021; Thieringer et al., 2023). Those that are primarily found in Type II fluids have evolved to replace H_2-dependent biochemical reactions with those dependent on formate. This has allowed cells to generate cytoplasmic CO_2 (through formate oxidation), an adaptation that effectively allows them to overcome carbon limitation by leveraging hydrogenated CO_2 (formate) that is likely also generated via serpentinization. Further, deeply branching H_2-dependent acetogens such as *Acetothermia* are also common in the serpentinite-hosted fluids and possess distinct metabolic pathways that reflect substrate availability differences in Type I vs. Type II fluids (Colman et al., 2022).

Thermodesulfovibrionia, a class of sulfate reducing organisms within the bacterial phylum Nitrospirota that can couple H_2 oxidation to sulfate reduction to generate energy for autotrophic growth, are also abundant in Samail ophiolite waters and, at times comprise more than 90% of the detected DNA sequences (Nothaft et al., 2021a; Templeton et al., 2021). Sequences affiliated with *Thermodesulfovibrionia* comprised ~50% of the metagenomic sequence recovered from deep (108–132 m), Type II waters, but only comprised <10% of metagenomic sequence in shallower (<65 m), Type II waters in a borehole in the Samail ophiolite, suggesting preferential inhabitation of deeper, more reduced waters (Munro-Ehrlich et al., 2023). Other genera of sulfate reducers such as *Desulfonatronum sp*. have also been detected in Samail ophiolite subsurface waters (Rempfert et al., 2017; Munro-Ehrlich et al., 2023). Groundwater sulfate concentrations vary from 10s of micromolar to 1 mM concentration (Nothaft et al., 2021b). Potential sulfate reduction rates have also been measured using sulfate radiotracer-based methods in the fluids (Glombitza et al., 2021) and rocks (Templeton et al., 2021), with rates varying from 0.001 to 2.1 pmol/cm^3/day. These are very slow rates, comparable to the slow sulfate reduction rates measured in deep marine sediments, with sulfate reduction rates in the ophiolite most suppressed at higher pH > 10.5. In the work by Glombitza et al. (2021), sulfate reduction rates were not significantly stimulated by addition of dissolved hydrogen, at least over short time-periods (e.g., 10 days), suggesting other factors might limit the rates of biological sulfate reduction activity. Nevertheless, sulfate reduction is widespread and persistent in the subsurface aquifer, resulting in the production of sulfide that reacts with the surrounding serpentinite matrix. The sulfur addition leads to optical darkening of the rocks and the formation of secondary sulfides (Kelemen et al., 2021; Templeton et al., 2021).

Evidence for denitrification, or the reduction of NO_3^- to N_2, and nitrate ammonification, or the complete conversion of NO_3^- to NH_3, is also common in the Samail ophiolite (Rempfert et al., 2017; Rempfert et al., 2023). All available dissolved NO_3^- introduced into the aquifer through rainwater is consumed, which can sometimes reach values as high as 366 micromolar in Type I groundwater fluids, potentially giving rise to a substantial production of NH_3 (up to 115 micromolar) that accumulates in the more hyperalkaline and reducing Type II fluids (Rempfert et al., 2023). Consistent with this notion, protein encoding genes required for denitrification are common in Type I fluid communities (Rempfert et al., 2023). While denitrifiers are most commonly associated with heterotrophic metabolisms, this group of organisms often supplement their heterotrophic metabolism with H_2 (Greening et al., 2016).

Most notably, the microbial community structure and function are strongly shaped by differences in groundwater chemistry, particularly the differentiation between Type I and Type II fluids (Rempfert et al., 2017; Fones et al., 2019; Colman et al., 2022). The high dissolved hydrogen concentrations that reach millimolar levels in hyperalkaline Type II fluids co-occur with low carbon and oxidant availability, severely limiting H_2-consuming microbial activity. In

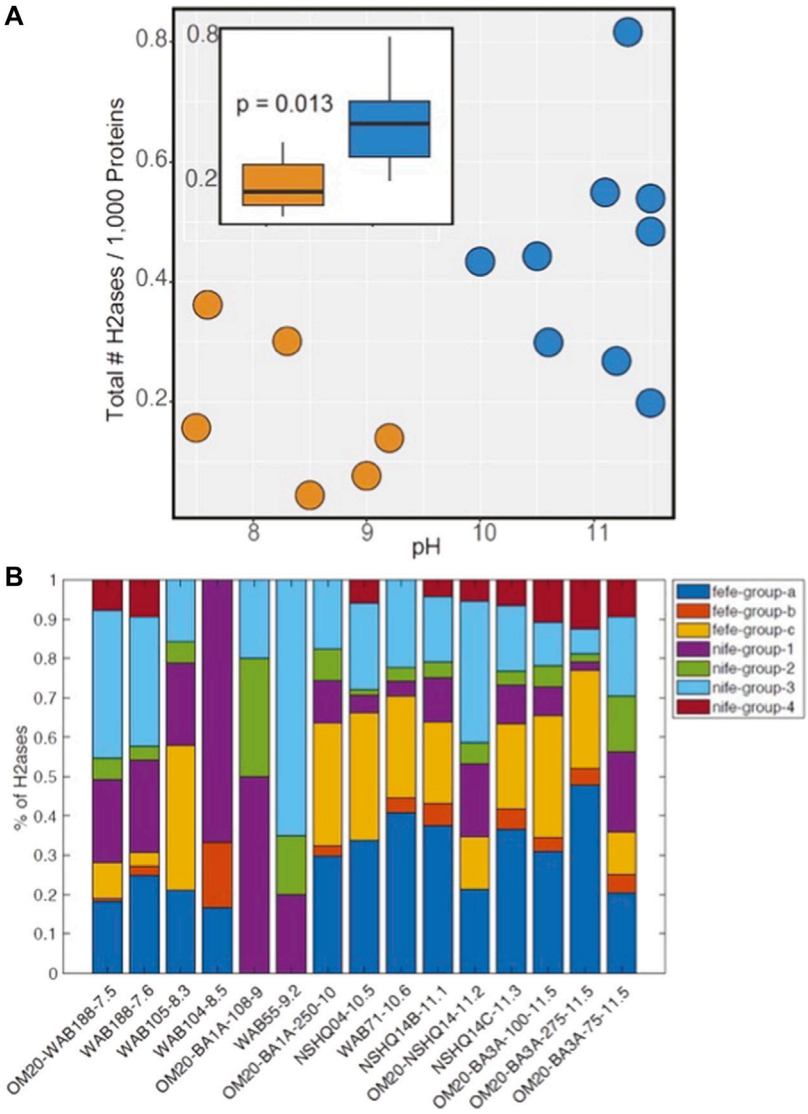

FIGURE 3
(A) Abundance of [NiFe]- and [FeFe]-hydrogenase encoding genes in 15 community metagenomes generated from DNA recovered from subsurface waters in the Samail Ophiolite. Each point represents a single metagenome and are color coded according to the pH of the waters from which the DNA was recovered. The inset shows a boxplot of the relative abundance of hydrogenase homologs, with the interquartile ranges of distributions denoted by the boxes and medians shown as black lines in the center of the boxes. Whiskers show the full ranges of the distributions. The metagenomes were grouped according to pH realms and are colored orange (pH <10) and blue (pH >10) and the *p*-value derives from a Kruskal-Wallis test. **(B)** Relative abundance of [NiFe]- and [FeFe]-hydrogenase phylogenetic groups among the same 15 community metagenomes. The metagenomes are organized from left to right based on the pH of the waters from which they derive, as indicated by the number following the metagenome ID.

contrast, H_2 is below a 10 nanomolar detection limit in the more oxidizing Type I fluids, suggesting a high capacity for microbiomes to consume the gas. This >5 orders of magnitude decrease in dissolved H_2 concentrations is strongly controlled by a combination of the hydrology (i.e., fluid mixing in fractures) and blooms of biological activity where suitable electron donors (i.e., H_2) and electron acceptors (e.g., nitrate, oxidized sulfur, CO_2) co-occur. The resulting consumption likely leads to the very low levels of H_2 outgassing observed at the surface, which will instead be restricted to fault zones that can transmit Type II fluids to surface springs and seeps without significant mixing with Type I fluids prior to discharge.

2.6 Abundance of hydrogenase enzymes

The protein catalysts (e.g., enzymes) that microorganisms use for the reversible oxidation of H_2 are termed hydrogenases (Vignais et al., 2001; Peters et al., 2015; Greening et al., 2016; Boyd et al., 2024). Publicly available community metagenomes from subsurface fluids in the Samail ophiolite were compiled to investigate the abundance of both [NiFe]- and [FeFe]-hydrogenases, which are forms of the enzyme that have diversified to allow for coupling with diverse oxidants including oxygen, nitrate, ferric iron, sulfate, and carbon dioxide (acetogenesis, methanogenesis) (Boyd et al., 2014) (Supplementary Table SB1). Communities from Type II waters

(pH >10.0) encoded on average, 2 times as many hydrogenase encoding genes per 1,000 protein encoding genes sequenced, when compared to those from Type I waters (pH <10) (Figure 3A; p = 0.013 using the Kruskal Wallis test). On average, 66% (range of 43%–88%) of metagenome assembled genomes (MAGs) from Type II waters encoded a homolog of a [NiFe]- and/or [FeFe]-hydrogenase, whereas 38% (range of 12%–73%) of MAGs from Type I waters similarly encoded hydrogenase homologs (Supplementary Table SB2). Roughly 30% of archaeal and bacterial genomes in a database compiled in 2015 (Peters et al., 2015) encode a homolog of a [NiFe]- and [FeFe]-hydrogenase, indicating that populations from both Type I and II waters are especially poised to metabolize H_2 relative to average archaeal or bacterial organisms.

The hydrogenase homologs were further classified into phylogenetic groups, which allows for the prediction of the directionality of the enzymes (Peters et al., 2015; Søndergaard et al., 2016; Boyd et al., 2023). For example, group 1 and 3 [NiFe]-hydrogenases tend to function in H_2 oxidation, whereas group 2 [NiFe]-hydrogenases enzymes tend to function either oxidatively or as H_2 sensors. Group 4 enzymes function reversibly, with the directionality dependent on the energy state of the cell (Lie et al., 2012). In the case of [FeFe]-hydrogenase homologs, the homologs were grouped based on whether they belong to prototypical [FeFe]-hydrogenases that can be involved in fermentation, H_2 oxidation, and/or those that bifurcate electrons from H_2 (group a), in addition to those with currently unresolved function (groups b and c). Comparing the relative abundance of hydrogenase groups among the 15 metagenomes from subsurface communities in the Samail ophiolite revealed an increased prevalence of [FeFe]-hydrogenase encoding genes in communities from Type II waters (Figure 3B). The prevalence of group 4 [NiFe]-hydrogenases was also higher in communities from Type II waters. Taxonomic profiling of the genomes from which these protein encoding genes were derived (Supplementary Table SB3) indicated that they were associated with methanogenic archaea affiliated with *Methanobacterium*, putative hydrogenotrophic sulfate reducers (e.g., *Desulfonatronum*), and the bacterial acetogens within *Acetothermia*, among many other uncultured taxa (Supplementary Table SB3), consistent with previous studies documenting the increased prevalence of these groups in Type II waters (Rempfert et al., 2017; Fones et al., 2019; Nothaft et al., 2021b; Kraus et al., 2021; Templeton et al., 2021; Colman et al., 2022; Munro-Ehrlich et al., 2023; Thieringer et al., 2023).

The increased prevalence of hydrogenase homologs in communities inhabiting Type II waters versus Type I waters, could be attributed to an excess flux of electron acceptors in Type I waters relative to H_2, an excess of H_2 relative to electron acceptors in Type II waters, or due to limitation of other key nutrients (e.g., carbon or phosphorous) in Type II waters that otherwise limits overall microbial activity. The results indicate that microbial communities that inhabit Type II waters are highly adapted to leverage the availability and abundance of H_2 in those systems and are likely poised to consume a substantial amount of H_2, should other limiting factors be relieved. Another possibility afforded by the observed increased prevalence of the reversible group 4 [NiFe]-hydrogenase homologs and [FeFe]-hydrogenase homologs likely involved in fermentation in Type II waters is that they are contributing to H_2 production in these systems through fermentative type reactions.

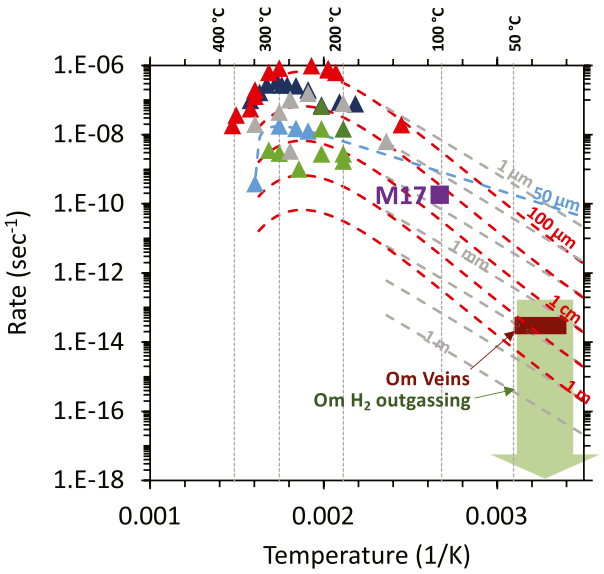

FIGURE 4
Summary of high-temperature laboratory- (triangles) and field-determined alteration reaction rates (green and red boxes) along with low temperature fits to results of high-temperature laboratory experiments. Figure is modified from Leong et al. (2023). The red dashed curves, accounting for varying surface areas, are low-temperature fits derived by Kelemen and Matter (2008) from the experiments of Martin and Fyfe (1970). The dashed blue and grey curves are fits derived by Malvoisin et al. (2012) and Lamadrid et al. (2021, for various indicated surface area or fracture spacing) from their own experimental data. The maximum estimated rate calculated from the experiments of Miller et al. (2017) is depicted by the violet square. Triangle symbols are results of high temperature experiments (>150°C): red—Martin and Fyfe (1970); dark blue—Wegner and Ernst (1983); light blue—Malvoisin et al. (2012); light green—McCollom et al. (2016); dark green—McCollom et al. (2020a); grey—Lamadrid et al. (2021) calculated for a 10 µm grain size.

2.7 Conceptual model for the processes controlling the net flux of hydrogen from Oman peridotites

2.7.1 Production rates

The rate at which hyperalkaline fluids and reduced volatiles are generated during low-temperature serpentinization is poorly known. Often, reaction rates are predicted from the rate at which H_2 is generated at high temperature and pressures in hydrothermal experimental water/rock reaction systems. Experiments simulating serpentinization at high temperatures (150°C–300°C, see Figure 4) yield the fastest serpentinization rates (Martin and Fyfe, 1970; Wegner and Ernst, 1983; Okamoto et al., 2011; Lafay et al., 2012; Malvoisin et al., 2012; Andreani et al., 2013a; Ogasawara et al., 2013; McCollom et al., 2016; McCollom et al., 2020a; McCollom et al., 2020b; Lamadrid et al., 2021). As shown in Figure 4, rates derived from high-temperature experiments are highly variable, spanning up to four orders of magnitude at a given temperature (also see Barbier et al., 2020; McCollom et al., 2016 for discussion). Then

these rates are extrapolated to lower temperature, by assuming that the same reactions are operating from 25°C to 300°C. When high-temperature rates are extrapolated to low temperature conditions, the range of predicted rates is again highly variable (Figure 4), and highly dependent on whether the fits are based upon the fast rates observed in the experiments of Martin and Fyfe (1970), Andreani et al. (2013a) and Lafay et al. (2012), or fits calculated by Malvoisin et al. (2012) or Lamadrid et al. (2021) from their slower experimental results.

Alternatively, rates can be estimated from experiments conducted at lower pressures and temperatures ≤100°C, which differ significantly from high P and T experiments (Barbier et al., 2020), although such experiments are rare. Using partially-hydrated Oman peridotite as the protolith, Miller et al. (2017) measured up to 470 nanomole of H_2 generated per gram of reactant after 97 days of reaction at 100°C. Assuming that the reactants (serpentinized Oman dunite) used in the Miller et al. experiment has ~8 wt% FeO and generation of a mole of H_2 requires oxidation of 2 moles of FeO, this corresponds to a mass fraction reaction rate of ~10^{-10} sec^{-1}. The maximum rate estimated from the low-temperature (100°C) experiments of Miller et al. (2017) is consistent with low-temperature fits from high-temperature experiments (see violet triangle in Figure 4). The average reactive grain size was 100 microns (Miller et al., 2017), and the inferred grain-size from the extrapolations is ~30 μm to ~3 mm, depending on the choice of high temperature experimental data and the extrapolation method fit (Figure 4).

Leong et al. (2023) recently provided estimates of rates of the low-temperature serpentinization and H_2 generation rates in the Samail ophiolite based upon field measurements of H_2 outgassing rates measured from several bubbling spring sites in Oman. The maximum subsurface reaction rate estimated by Leong et al. (2023) of 8×10^{-14} sec^{-1} is similar to the $3x10^{-14}$ sec^{-1} rate estimated from in Oman Drilling Project drill cores (Kelemen et al., 2021). In the cores, 23 out of 35 samples of carbonate veins contained appreciable ^{14}C and thus, contained a relatively young carbon component. These carbonate veins are intergrown with and cut by a generation of "waxy serpentine" veins comprising ~1% of the drill cores. This leads to an order-of-magnitude serpentinization rate of 1 volume percent per 10,000 years. Assuming no large density contrast, this is equivalent to a mass fraction rate of $3x10^{-14}$ sec^{-1} (red rectangle in Figure 4). Overall, these field-based serpentinization rates estimated for the Oman ophiolite are consistent with those extrapolated from high-temperature experiments, assuming low reactive surface area, with a reactive grain size or fracture spacing >1 cm.

2.7.2 H_2 consumption rates

We can conduct a back-of-the-envelope calculation to estimate the scale of microbial H_2 consumption in the peridotite aquifers. Cell counting conducted with the serpentinite rocks recovered through the Oman Drilling project enables us to establish a conservative 10^5 cells/cm^3 average in the bulk rock, which is equivalent to serpentinized peridotite containing 10^{20} cells/km^3 (Templeton et al., 2021). Given the low abundance of other electron donors relative to H_2 or CH_4, and little evidence for methanotrophic activity, we will assume 50%–100% total population is dependent on H_2 as an energy source for growth, depending upon which part of the system is under examination. The next assumption we make is that 1 mol of H_2 can support the biomass production of 10^{14} cells. This estimate is derived from analysis of energy limited methanogens, which can produce $(0.2–0.5)*10^{14}$ cells/mol H_2 (Chen et al., 2019), and more energy replete H_2-driven denitrifiers, which can produce >10^{14} cells/mol H_2 (Strohm et al., 2007). Thus, for a standing biomass of 10^{20} H_2-consuming cells/km^3 rock, we estimate 10^6 moles H_2/km^3 was consumed for lithotrophic growth.

The next question is the rate of H_2 consumption required to maintain the populations of microorganisms inhabiting the peridotite, which is currently unknown. In rock-hosted systems, the cellular turnover rates may vary from days to 10s or 100s of years (Templeton and Caro, 2023). For this thought exercise, if we assume an average of 1 turnover per cell per year, we can infer the microbial consumption to be 10^6 moles H_2/km^3/year, which is equivalent to 2 tonnes H_2/km^3/year. This conservative calculation shows a remarkable correspondence with the maximum of 4 tonnes H_2/km^3/year H_2 production rates estimated by Leong et al. (2023). If cells are more abundant, or turning over faster than once per year, then the rate of microbial consumption will increase by at least one or more orders of magnitude and significantly exceed the predicted production rate. Since consumption cannot exceed the available H_2 produced during serpentinization, the biological system is likely highly tuned to the prevailing H_2 production rate. Therefore, constraining the cellular turnover rates will be valuable information to obtain.

To check these preliminary estimates, we can also quantify predicted H_2 production through calculations that more closely follow the approaches laid out in Hoehler et al. (2023) in their assessment of the metabolic rate of the global biosphere. In this case, if we use an average of 10^5 anaerobic cells/cm^3 and assume this biomass replaces itself with one turnover per year, as above, we can then use energy requirement from Hoehler et al. (2023) and the H_2-requirement for methanogenesis to yield an estimate of almost 4 tonnes of H_2/km^3/yr (see Supplementary Material for calculation details). This estimate would also scale to a larger H_2 consumption rate if the cell abundance or turnover rates are increased. On the other hand, total amount of H_2 required would decrease if the most energetic metabolisms (e.g., denitrification) were utilized, due to the lower amount of H_2 required to produce the same amount of energy.

The maximum potential H_2-consuming activity of the peridotite-hosted biosphere is likely enormous. In addition to the calculations provided here so far, Boyd et al. (this issue) have predicted that the habitable volume in the peridotite may exhibit H_2-consumption rates as high as 52,000 tonnes/km^3/yr, based upon comparison of the system characteristics (temperature, porosity) to other H_2-dominated ecosystems such as glacial basalt and carbonate sediments, subsurface clays, and hot-spring sediments that vary in temperature from 0 to 70°C. This order of magnitude increase in the estimated H_2 consumption rate is agreeable with the others reported above, considering potential turnover times could be far faster than once per year (e.g., week to month turnover times).

Our inference based on these data and calculations is that H_2 production and consumption are relatively balanced over the scale of the hydrologically-active zone. Within this conceptual model we should add some complexity to encompass a prediction that higher levels of microbial activity in the shallow aquifer are sustained by a flux of H_2 produced at greater depth (Figure 5). Under the more

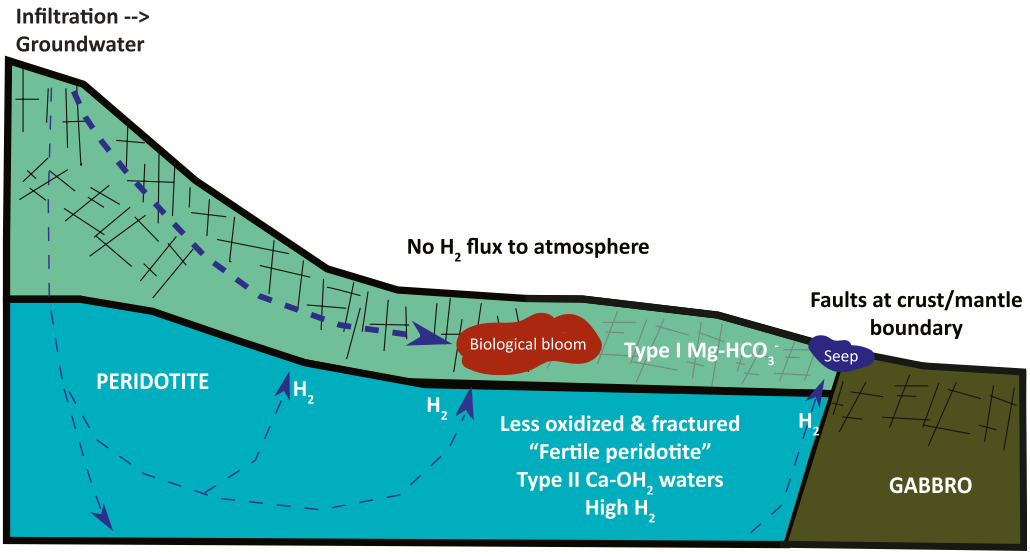

FIGURE 5
Conceptual figure of the distinct subsurface biogeochemical regimes. A deeper reaction zone at low water/rock conditions produces net H_2 from the oxidation of Fe(II)-bearing peridotite, despite the presence of microorganisms functioning under extreme carbon and oxidant limitation. In contrast, in the more shallow, oxidant replete aquifer, biological activity is predicted to be stimulated by fluxes of H_2, giving rise to net H_2 consumption. The most probable detection of H_2 at the surface is at hyperalkaline seeps sourced by deep faults, rather than in most soils and peridotite outcrops, due to efficient microbial H_2 scavenging of the available H_2 flux in the upper aquifer, where measured $H_{2(aq)}$ levels drop below detection.

hyperalkaline, closed system conditions that prevail through most of the deeper hydrating rock volume, there is evidence of less extensive hydration and alteration (Kelemen et al., 2020, 2021; Ellison et al., 2021), giving rise to rocks "fertile" for H_2 production. Simultaneously, microbial activity is predicted to be suppressed due to carbon limitation and the higher pH in these deeper rock hosted fluids (Fones et al., 2019, 2022; Glombitza et al., 2021; Templeton et al., 2021), and some biological activity may even contribute to H_2 production. Here hydrogen production will be favored over microbial consumption. The produced hydrogen will either be trapped and stored in nanoporosity, or be transported to the shallower parts of the aquifer where more oxidizing conditions prevail. In contrast, we predict H_2 production rates are low in the shallow aquifer in the upper 100–200 m, because the rocks are almost fully serpentinized and oxidized (Kelemen et al., 2020, 2021; Ellison et al., 2021). Instead, H_2 is delivered through a combination of advective mixing and diffusive fluxes. Here Type I fluids prevail and there is greater oxidant availability and microbial H_2 consumption rates and turnover times should be significantly increased. Thus, consumption will exceed local production in these shallow aquifers (see Figure 5). In mixing zones with the highest chemical disequilibrium between Type I and Type II fluids, biological blooms are likely occur (Leong and Shock, 2020; Howells et al., 2022; Templeton and Caro, 2023). The system should be relatively "silent" at the surface, without significant H_2 flux to the atmosphere, because of the excess of oxidants available to support microbial consumption of any H_2 that fluxes into the upper aquifers. Thus, we infer that the only measurable gas flux to the surface is along the fault zones that transport fluids from deeper reaction zones to surface seeps in conduits with high fluid/rock ratios, at flow rates faster than microbial consumption rates (e.g., Leong et al., 2023).

These predictions can be tested by doing future work to directly measure how the microbial H_2 consumption rates, cell abundances and cellular turnover-times change as a function of the varying Eh-pH conditions in the aquifer(s). Building a quantitative model constrained by such data from rock cores and fluids will provide valuable insights into the scale and structure of the H_2-producing reaction zones vs. the H_2-consuming zones and how they together regulate net H_2-production under the current *in-situ* conditions. In addition, by coupling H_2-activity measurements with measurements of the utilization of specific oxidants (e.g., CO_2, sulfate, nitrate and ferric minerals), and quantifying how their different energetic yields affect cellular turnover rates, we can further constrain the relative importance of specific metabolisms in regulating microbial H_2 consumption. These insights will be essential to guide future efforts to change the balance of H_2-production vs. consumption as part of engineering stimulated H_2 production to increase the net H_2 flux by several orders of magnitude.

3 Concepts, challenges and opportunities for stimulated geological hydrogen in Oman

3.1 Why Oman?

The Samail ophiolite in Oman is the largest subaerial exposure of lower crustal and upper mantle rocks on Earth (Nicolas et al., 2000). The ultramafic rocks in the mantle section comprise a volume of ~10,000 km^3 dominated by harzburgite, with up to 15% dunite (Boudier and Coleman, 1981). Finding a way to sustainably harness some of the abundant peridotite resources could position Oman to become a global leader in stimulated hydrogen production, should

this prove to be an environmentally and economically feasible process. For example, more than 200 Mt of hydrogen could potentially be produced if 100 km^3 of suitable rocks could be identified for stimulation, which is ≤1% of the total peridotite estimated to be present across the ophiolite. Given that every 1 Mt of hydrogen could produce 33 TWh and offset 23 million tonnes of CO_2 emissions, that is a substantial impact.

Assessing the hydrogen generation potential of subsurface Oman rocks first requires a detailed understanding of the mineralogy, FeO content and reservoirs of Fe(II) that can be converted to Fe(III) coupled to water reduction. Although fresh peridotite can theoretically produce 2–4 Mt H_2/km^3 (Osselin et al., 2022), the maximum yields will vary depending upon initial protolith composition, Fe-content, and the degree to which some of the initial FeO component has already been oxidized by prior water/rock reaction. For example, the average FeO component of the rocks is 8% (Godard et al., 2000; Monnier et al., 2006; Hanghøj et al., 2010). Oman harzburgites and dunites characterized using X-ray spectroscopic techniques to quantify the Fe-speciation have shown that more than 40% of the Fe has already been oxidized through prior water/rock reaction (Mayhew et al., 2018). However, given the high Fe content of the peridotite, there is still a substantial reservoir of reactive Fe(II) that can be utilized in stimulated H_2-producing reactions. Much of the Fe(II) has been stabilized under the prevailing low water/rock reaction conditions at depth, but once fluids are introduced, significant H_2 production should ensue under high water/rock ratio, more open system conditions, so long as excess alternative oxidants are not present.

Stimulated hydrogen production could be integrated into the development of a hydrogen strategy in the Sultanate of Oman. Oman Vision 2023 (the Oman National Energy Strategy; 2023), and the *Oman National Strategy for an Orderly Transition to* Net Zero (2022) together establish a path to a low-carbon economy, in part through the development of renewable energy resources. In addition, it is anticipated that the Sultanate of Oman will adopt the use of more low-carbon hydrogen in the near future. The Ministry of Energy and Minerals recently signed an agreement with stakeholders from the oil and gas industry to establish a regulatory framework for hydrogen produced from steam reforming of natural gas (i.e., "blue hydrogen"; Ministry of Energy and Minerals Supports Studies of the Proposed Shell-Led Blue Hydrogen and Ammonia Project, 2023), coupled with carbon capture, utilization and storage. Oman is also in the process of developing an infrastructure for the production, storage, transport and use of hydrogen produced through electrolysis. Such efforts have included the establishment of the state-owned company Hydrom (https://hydrom.om), which supports the development of "green-hydrogen" projects (i.e., production of hydrogen by electrolysis of water using renewable electricity sources) and the associated allocation of land and development of required infrastructure.

There may also be the potential for natural hydrogen accumulations that could be harnessed as an energy source in Oman. For example, there may be reservoirs of hydrogen previously generated by serpentinization, and then accumulated over 10s of millions of years beneath low permeability clay-rich caprocks overlying the Samail ophiolite, which have been seismically imaged along the northeastern coast of Oman (Ninkabou et al., 2021). However, such an assessment is beyond the scope of this work.

3.2 Preliminary technoeconomic perspectives

There is great interest in identifying sources of geological hydrogen that will be competitive on the global market. Recently, the U.S. Department of Energy set targets of achieving a cost of <$1/kg at the wellhead, and without significant greenhouse gas emissions (<0.45 kg CO_2/kgH_2). The U.S. DOE also set targets of >10 MtH_2 produced per deposit, which would require stimulating and fully exhausting the H_2 potential of at least 5–10 km^3 of peridotite in a system similar to Oman (assuming 1–2 Mt H_2/km^3 maximum yield for these specific rocks), and >300,000 tonnes of H_2 produced per year per deposit.

We have independently examined some of the assumptions about the H_2 production rates that may be required for stimulated geological H_2 to be economically feasible in Oman, and we address some of the technical challenges that will be associated with such efforts below. We acknowledge that the potential profitability of stimulated geological hydrogen production is highly unconstrained, and is subject to a large number of variables. These variables include natural rates of hydrogen production, reservoir characteristics [e.g., permeability, reactive surface area, reactivity of Fe(II) phases], and engineering decisions (e.g., depth of injection and production wells, source of water, costs of drilling and operations). Furthermore, the potential stimulation methods need to be defined, and therefore their potential effectiveness is currently unknown.

To explore the parameter space and assess the interplay between hydrogen production rates, reactive surface area, and magnitude of stimulation that would be required to achieve profitability, we created a simple interactive model of the hydrogen production process and the costs involved. The model allows the user to explore the effects of changes in the various unconstrained parameters (Ellison, 2024). It is available online at https://ericellison.shinyapps.io/gain_loss/, and the associated details of the model calculations are provided in the Supplementary Material.

An example of output from our interactive model is illustrated in Figure 6. The calculations have been conducted for fertile peridotite containing at least 4.5 wt% reactive FeO (FeII) component that in a small stimulation volume that is 500 m deep and 50 m wide, between injection and production wells that are 100 m apart (i.e., the stimulation volume is 0.0025 km^3). This chosen FeO component (4.5%) acknowledges that a significant fraction of the original 8 wt% FeO in the peridotites is already oxidized due to prior water/rock reaction, even in deeper rocks that have not experienced high water fluxes and associated weathering at shallower depths. The heatmap in the background indicates combinations of H_2 production rates and reactive surface areas that would be profitable (colors) or not profitable (gray). A selection of published reaction rate data for experiments with finely crushed olivine, forsterite + pyroxene, or serpentinite rocks, at relatively low temperature (≤150°C) are included (Martin and Fyfe, 1970; Lafay et al., 2012; Miller et al., 2017). Additionally, rates extrapolated from the experimental results of Martin and Fyfe (1970) to lower temperatures using the fit by

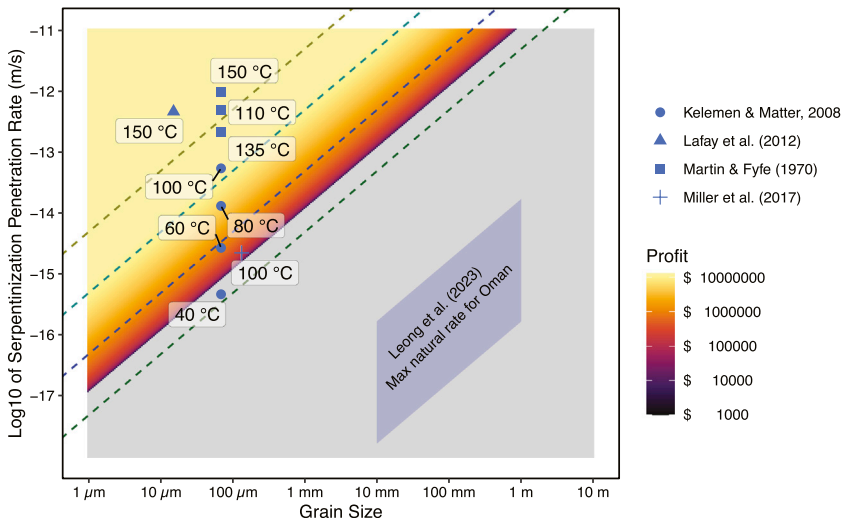

FIGURE 6
Potential profitability of a small (0.0025 km^3) hypothetical stimulated geological H_2 production operation as a function of the serpentinization rate and effective grain size, modeled according to the methods described in SI. Only capital ($600K) and operational ($200K/yr) costs to get H_2 to the well-head are considered, with assumptions of a 15-year operation, with a H_2 market price of $5/kg. The lowest temperature experimental data (Martin and Fyfe, 1970; Lafay et al., 2012; Miller et al., 2017), together with extrapolations to even lower temperatures (Kelemen and Matter, 2008), are plotted with temperatures annotated. Maximum natural H_2 production rates in Oman inferred from surface flux measurements are also shown (Leong et al., 2023).

Kelemen and Matter (2008), as well as the maximum estimated natural H_2 production rate in Oman based on H_2 flux measurements at the surface by Leong et al. (2023) are overplotted.

In the example results of Figure 6, the model output shows that if subsurface rocks could react at rates close to those derived from laboratory experiments, which used finely pulverized ~100 μm olivine or peridotite samples, this would be fast enough to be profitable under the model assumptions. However, these are extremely rosy predictions! The reactive surface area in the subsurface serpentinite is much smaller, perhaps corresponding to fracture spacing of 10 mm–1 m (Leong et al., 2023), which means that even if the same hydration and oxidation rates observed in experiments are achieved in the natural system, once scaled to the available reactive surface area, the H_2 production will be several orders of magnitude too slow for profitability. Thus, it is likely that significant stimulation will be required.

In comparing the estimated natural rates from Leong et al. to the "profitable zone" in Figure 6, we find that the net H_2 production rates need to be increased by $\geq 10^4$. It will be essential to either move "up" from the Leong et al. (2023) predictions by a direct increase in the reaction rate, or to move "left" on the diagram by decreasing the fracture spacing and effective grain size. These required rate increases may possibly be accomplished through a combination of mechanisms described in Section 3.3.

In assessing the model, we acknowledge significant concerns about the investment costs of stimulated geological hydrogen, which deserve detailed investigation and a robust technoeconomic analysis for each possible geological scenario. In this preliminary analysis for the Samail Ophiolite, we use cost estimates that are far lower than might be assumed, for example, in North America, where drilling costs will be >$150,000/day, or in offshore environments that would be substantially more expensive to drill. Fortunately in Oman, we start by assuming it will be feasible to stimulate hydrogen production in reaction volumes located at less than 1 km depth in sufficiently fresh peridotite. Using our experience in drilling wells and conducting borehole experiments in the Samail Ophiolite, we envision capital investment costs that could be as low as $600K for permitting, construction of access roads, drilling completion of injection, production and paired monitoring wells, and the installation of required infrastructure for fluid injection and extraction. This is coupled with estimated annual operational costs of $200K/year for providing required water and energy, plus the personnel costs of maintaining a small operation. We have not investigated costs post-delivery to the well-head, such as gas-separation, storage or transport.

3.3 Approaches to stimulation

Stimulating geological H_2 production will involve chemical, biological, mechanical or thermal perturbations that increase the rate of H_2 production and/or decrease loss. Such methods will likely need to be applied in combination to achieve the required 4-5 orders of magnitude increase in the hydrogen yield.

Several potential strategies for stimulating geological hydrogen production can be considered for Oman. At the highest level, stimulation must start by increasing the water/rock ratio. This can be accomplished through fracturing of target rocks using hydraulic or electrical methods followed by the injection of fluids into new fractures to drive increased

serpentinization of the peridotite. For a system like the Samail Ophiolite, where pre-existing, mineralized fractures already exist down to the 50 micron scale (Dewandel et al., 2005), it will also be important to assess whether such interfaces can be re-activated and kept open to fluid flow. By achieving a reduced fracture spacing, and thus a smaller effective grain size with a larger reactive surface area, the system will be able to move to the "left" on Figure 6, giving rise to greater H_2 production rates per volume of rock. The key variables to be assessed at the field scale are the extent of new fracture surface area that is produced, changes in the effective grain size, and the ability to distribute the fluid through the fracture network rather than short-circuiting of flow, via focusing in a few dominant fractures. The water/rock ratio can then be further optimized by controlling the rate of injection and fluid extraction.

A deeper understanding of reaction-driven cracking processes would be beneficial. Reaction-driven cracking can occur when the thermodynamically-favorable rock hydration and oxidation, and associated volume increase, occurs rapidly, creating high differential stresses. Fracturing can occur at multiple scales, including scales on the order of 10s–100s of microns (Iyer et al., 2008; Jamtveit et al., 2008; Rudge et al., 2010; Kelemen and Hirth, 2012). If conditions can be optimized to initiate reaction-driven cracking and sustain infiltration of fluids into existing fractures, the resulting self-propagation of the fracture network may refresh the permeability and the reactive surface area, which is essential to mitigating possible surface passivation over time and clogging of fluid flow pathways during secondary mineralization. Reaction-driving cracking is likely required to fully serpentinize and oxidize the target olivine and pyroxene rich formations.

From here, additional mechanisms of stimulation can be explored. For example, the rate of serpentinization and hydrogen production will increase with temperature. The temperature can be increased by 1) drilling deeper, following the geothermal gradient of ≥20°C/km (Kelemen et al., 2021), 2) heating the shallower formations through inputs of external energy, or 3) exothermic heating during mineral hydration reactions (Kelemen and Matter, 2008). However, the scale of exothermic heating will also be highly sensitive to the rates of fluid injection and circulation. Models need to carefully account for these interactions, and they must include an assessment of the energy costs and CO_2 footprint associated with heating of the rocks.

Further pathways to stimulation require careful testing in the field and in the laboratory. Although the rates of hydrogen production have proven to vary by orders of magnitude in laboratory experiments conducted at similar temperatures, grain sizes and fluid compositions, it has been difficult to determine what controls this variability. Changes in serpentinization rates can be sometimes attributed to which reactions regulate silica activity (McCollom et al., 2020a), or specific ion activities, such as $Al^{3+}_{(aq)}$ (Andreani et al., 2013a), Ni^{2+} (Song et al., 2021), other fluid variables such as salinity and pH (Lafay et al., 2012; McCollom et al., 2020b), or enhanced electron transfer by specific mineral phases such as spinels (including magnetite or chromite), metal alloys or Ni sulfides (Mayhew et al., 2013; Barbier et al., 2020). Thus there is significant ongoing experimentation being conducted in research laboratories worldwide that is focused on optimizing the mechanisms of catalysis and the chemical factors that may increase net H_2 yields. New experiments and modeling efforts have also been initiated to investigate whether serpentinization and H_2 production rates are controlled by rates of olivine and pyroxene dissolution, and can be modeled using temperature dependent rates derived from compilations such as Oelkers et al. (2018), or whether they are more controlled by secondary mineral formation as the rate determining step for the overall serpentinization process (Nesbitt and Bricker, 1978).

It is worth noting that most experiments have focused on the high temperature alteration of olivine to magnetite, brucite and serpentine, and many fewer have been conducted with the complexity of a full peridotite composition, which exerts an enormous control on the predicted H_2 yields (Ely et al., 2023). Thus stimulating hydrogen production requires much more attention to promoting the secondary mineralization pathways that yield the most H_2 under the *in-situ* conditions found in the Oman peridotite aquifers (Leong et al., 2021b). In particular, it will be essential to understand controls on the partitioning of Fe(II) and Fe(III) into secondary phases such as serpentine, magnetite and hydroandradite, and how to promote the rapid formation of ferric phases coupled to the reduction of water to H_2.

In addition, it will be important to understand and control the timing of hydrogen generation. In many experiments, serpentinization rates and associated hydrogen production rates often experience a notable lag during incipient alteration (Seyfried et al., 2007; Grozeva et al., 2017; McCollom et al., 2020a). Significant reaction with fresh protoliths may need to occur until the fluids reach the more alkaline, low SiO_2 conditions conducive to H_2 production. In Oman, the mantle rocks have already experienced several episodes of prior water/rock interaction at varying temperatures (Noël et al., 2018; Scicchitano et al., 2020), and initial hydration products such as brucite and Fe(II)-rich serpentine have been formed at low water/rock ratios (Ellison et al., 2021; Kelemen et al., 2021). Therefore, in this system, we anticipate that phases such as metastable Fe(II)-bearing brucite will rapidly react with circulating fluids, producing a notable initial pulse of H_2 (e.g., Miller et al., 2017). Once the previously-formed brucite is exhausted, the overall H_2 production rate will become much more sensitive to the rate controls on olivine, pyroxene and Fe(II)-serpentine alteration to secondary Fe(III)-bearing phases.

Stimulating hydrogen production will also depend upon ensuring that H_2 production greatly exceeds the rate of microbial consumption. In turn, this will require that the fluid conditions in the reaction volume do not stimulate biological growth and increased activity. From prior interrogation of the system, the microbial communities are astoundingly resilient to low nutrient concentrations (e.g., phosphate) and high pH, showing activity, albeit at reduced rates, even at pH >10 (Fones et al., 2019; Glombitza et al., 2021; Kraus et al., 2021; Rempfert et al., 2023). Therefore, manipulating these environmental variables will likely not be sufficient. The most essential factor controlling microbial H_2-consumption will be the carbon and oxidant availability, which should be minimized to ensure that the system is primed for net H_2

production vs. consumption (see Section 2.6). Note that this is to some extent the opposite of injecting fluids with high pCO_2 to optimize solution-trapping and carbon mineralization for CO_2 storage.

Oman is one of the world's five most water-stressed countries, due to large withdrawals coupled with limited freshwater availability (Kuzma et al., 2023). This has been exacerbated by decreasing rainfall. Decreasing precipitation also leads to greater energy demands, to produce more freshwater via desalination, requiring almost 100 Kwh/m^3. Fortunately, purified water will not be required for stimulated geological hydrogen production. Serpentinization can proceed with a diversity of fluid compositions, including as seawater and wastewater. In particular, wastewaters loaded with organics may be beneficial to stimulating hydrogen production, if their introduction first consumes strong oxidants and then promotes anaerobic microbial fermentation activity that produces H_2, in addition to pushing the system to the low pO_2 suitable for hydrogen production.

Depending upon the exact fluid chemistry, parasitic H_2 consuming reactions can occur. For example, net H_2 production can be significantly diminished in fluids containing dissolved oxidants. Less hydrogen will be produced when oxic fluids are injected, since the FeO component of the rock will preferentially react with dissolved O_2, reducing the available Fe for H_2 production once low fO_2 conditions are obtained during water/rock reaction. Alternative oxidants such as nitrate, sulfate and CO_2 should also be minimized. In particular, production of CH_4 from microbial CO_2 reduction should be avoided. In addition, fouling can occur if sulfide is produced via microbial sulfate reduction during stimulation using a sulfate-rich fluid such as seawater.

Therefore, the chemistry of the fluids to be utilized must be optimized prior to injection to give rise to reducing potentials more favorable for the production of H_2 than its oxidation. This can be achieved by the coupled biological and chemical "tuning" of the system. Yet it will also be important to carefully ensure that exogenous components are not added to the subsurface aquifer that may be detrimental if they were to be released from the stimulated reaction volume into the surrounding aquifer. The design of the H_2-recovery also needs to be optimized so that hydrogen produced in the circulating groundwater is extracted prior to substantial advective or diffusive losses. Ideally, stimulation of peridotite at depth will preserve an overlying caprock with low permeability, beneath which newly produced H_2 can accumulate, and flow toward production wells. Above such a caprock, we consider it beneficial that in Oman, there would be Type I oxidizing fluids in the shallow aquifer well above the target H_2 production zones, which should ensure efficient microbial consumption of any inadvertent leaks of H_2 through the caprock, preventing release to the atmosphere.

During any type of proposed stimulation, it will be important to monitor possible negative perturbations to the environment. This will include possible changes in groundwater chemistry, particularly if the aquifers could be impacted by the type of injection fluid(s) to be used; changes in microseismicity that could be induced through targeted fracturing, as well as reactive-driven cracking; changes in microbial community structure and abundance, due to blooms of opportunistic organisms stimulated by the introduction of oxidants; changes in greenhouse gas flux to the atmosphere, whether H_2 produced in the stimulation or other gases, such as methane, that are produced by H_2-dependent microbial activity. Establishing a strong baseline of environmental monitoring data before and after stimulation and quantifying perturbations will be essential for the future safe design of stimulated geological hydrogen operations.

4 Conclusion

Currently the technology readiness level (TRL) for Stimulated Geological Hydrogen lies at TRL 4, using the criteria established for natural geological hydrogen by Gaucher et al. (2023), in that the previous characterization, monitoring and testing of the geology, hydrology, geochemistry, microbiology and H_2 in pre-existing wells and boreholes discussed herein provides a framework for validation in the natural environment. The next step is to move towards TRL 5, by testing whether active H_2 production processes can be stimulated at depth.

The concept of stimulated geological hydrogen may not be economically feasible in many locations globally, due to the challenges of producing H_2 in subsurface fractured rock aquifers at acceptable rates and market prices, given the anticipated capital and operational costs. However, the Sultanate of Oman is one of the most favorable geological locations to test and then scale stimulated hydrogen production due to the abundance of fertile Fe(II)-rich peridotite rocks that can be accessed near the surface. Therefore, we suggest that it would be beneficial to conduct a pilot study of stimulated hydrogen production in reactive peridotites in Oman as soon as possible, to determine if it is possible to engineer the required >10,000-fold increase in the rate of geological H_2 production. Such a pilot should begin with drilling, followed by careful characterization of core, fractures, microseismicity, downhole magnetic fields, pore fluids, microbial activity and H_2 flux to establish a robust set of background measurements against which changes can be measured. After characterization, rock fracturing technologies will be required to permit the injection of fluids tuned to accelerate H_2 production, decrease the effective grain size, and increase reactive surface area. A pilot should then include continued characterization of the physical, chemical, biological and thermal changes that occur within the partially-serpentinized peridotites due to increasing fluid circulation, and reaction with engineered fluid compositions. Detailed characterization of changes in the fracture network, rock properties, geochemistry and microbiology of borehole fluids, H_2 flux and seismic activity, during and after stimulation. Sidewall coring should be considered, to monitor mineralogical and biological changes in rocks surrounding the boreholes. Comprehensive monitoring will be important in validating any new models of stimulated *in-situ* H_2 production, and identifying controls on the balance of processes that generate and consume H_2.

Data availability statement

The original contributions presented in the study are included in the article/Supplementary Material, further inquiries can be directed to the corresponding author.

Author contributions

AT: Formal Analysis, Funding acquisition, Writing–original draft, Conceptualization. EE: Writing–original draft, Software, Methodology, Formal Analysis, Visualization, Conceptualization. PK: Conceptualization, Writing–review and editing. JL: Visualization, Formal Analysis, Conceptualization, Writing–review and editing. EB: Methodology, Writing–review and editing. DC: Visualization, Data curation, Writing–review and editing, Formal Analysis. JM: Writing–review and editing.

Funding

The authors declare that financial support was received for the research, authorship, and/or publication of this article. This work developing the hypothesis and theory has been supported by the Grantham Foundation for the Protection of the Environment, and relies in part upon data produced through the prior support of the NASA Exobiology program and the Oman Drilling Project.

Conflict of interest

The authors declare that the research was conducted in the absence of any commercial or financial relationships that could be construed as a potential conflict of interest.

The reviewer MG declared a past co-authorship with the author AT to the handling editor.

The authors declared that they were an editorial board member of Frontiers, at the time of submission. This had no impact on the peer review process and the final decision.

Publisher's note

Supplementary material

The Supplementary Material for this article can be found online at: https://www.frontiersin.org/articles/10.3389/fgeoc.2024.1366268/full#supplementary-material

References

Abrajano, T. A., Sturchio, N. C., Bohlke, J. K., Lyon, G. L., Poreda, R. J., and Stevens, C. M. (1988). Methane-hydrogen gas seeps, Zambales Ophiolite, Philippines: deep or shallow origin? *Chem. Geol.* 71, 211–222. doi:10.1016/0009-2541(88)90116-7

Abrajano, T. A., Sturchio, N. C., Kennedy, B. M., Lyon, G. L., Muehlenbachs, K., and Bohlke, J. K. (1990). Geochemistry of reduced gas related to serpentinization of the Zambales ophiolite, Philippines. *Appl. Geochem.* 5, 625–630. doi:10.1016/0883-2927(90)90060-I

Andreani, M., Daniel, I., and Pollet-Villard, M. (2013a). Aluminum speeds up the hydrothermal alteration of olivine. *Am. Mineralogist* 98, 1738–1744. doi:10.2138/am.2013.4469

Andreani, M., Muñoz, M., Marcaillou, C., and Delacour, A. (2013b). µXANES study of iron redox state in serpentine during oceanic serpentinization. *Lithos* 178, 70–83. doi:10.1016/j.lithos.2013.04.008

Bach, W. (2016). Some compositional and kinetic controls on the bioenergetic landscapes in oceanic basement. *Front. Microbiol.* 7, 107. doi:10.3389/fmicb.2016.00107

Bach, W., Paulick, H., Garrido, C. J., Ildefonse, B., Meurer, W. P., and Humphris, S. E. (2006). Unraveling the sequence of serpentinization reactions: petrography, mineral chemistry, and petrophysics of serpentinites from MAR 15°N (ODP Leg 209, Site 1274). *Geophys. Res. Lett.* 33, L13306. doi:10.1029/2006GL025681

Barbier, S., Huang, F., Andreani, M., Tao, R., Hao, J., Eleish, A., et al. (2020). A review of H2, CH4, and hydrocarbon formation in experimental serpentinization using network analysis. *Front. Earth Sci.* 8. doi:10.3389/feart.2020.00209

Barnes, I., and O'Neil, J. R. (1969). The relationship between fluids in some fresh Alpine-type ultramafics and possible modern serpentinization, western United States. *Geol. Soc. Am. Bull.* 80, 1947–1960. doi:10.1130/0016-7606(1969)80[1947:trbfis]2.0.co;2

Bonnemains, D., Carlut, J., Escartín, J., Mével, C., Andreani, M., and Debret, B. (2016). Magnetic signatures of serpentinization at ophiolite complexes. *Geochem. Geophys. Geosystems* 17, 2969–2986. doi:10.1002/2016GC006321

Boschetti, T., Etiope, G., and Toscani, L. (2013). Abiotic methane in the hyperalkaline springs of genova, Italy. *Procedia Earth Planet. Sci.* 7, 248–251. doi:10.1016/j.proeps.2013.02.004

Boudier, F., and Coleman, R. G. (1981). Cross section through the peridotite in the Samail ophiolite, southeastern Oman mountains. *J. Geophys. Res. Solid Earth* 86, 2573–2592. doi:10.1029/JB086iB04p02573

Boulart, C., Chavagnac, V., Monnin, C., Delacour, A., Ceuleneer, G., and Hoareau, G. (2013). Differences in gas venting from ultramafic-hosted warm springs: the example of Oman and Voltri ophiolites. *Ofioliti* 38, 143–156. doi:10.4454/ofioliti.v38i2.423

Boyd, E. S., Amenabar, M. J., Poudel, S., and Templeton, A. S. (2020). Bioenergetic constraints on the origin of autotrophic metabolism. *Philosophical Trans. R. Soc. A Math. Phys. Eng. Sci.* 378, 20190151. doi:10.1098/rsta.2019.0151

Boyd, E. S., Colman, D., and Templeton, A. S. (2024). Perspective: microbial hydrogen metabolism in rock-hosted ecosystems. *Front. Energy Res. Sec.* Sec. Hydrogen storage and production 12, 2024. doi:10.3389/fenrg.2024.1340410

Boyd, E. S., Schut, G. J., Peters, J. W., and Adams, M. W. (2014). Hydrogen Metabolism and the Evolution of Biological Respiration: two separate families of enzymes that oxidize hydrogen and also produce it arose through convergent evolution. *Microbe Mag.* 9, 361–367. doi:10.1128/microbe.9.361.1

Boyd, E. S., Spietz, R. L., Kour, M., and Colman, D. R. (2023). A naturalist perspective of microbiology: examples from methanogenic archaea. *Environ. Microbiol.* 25, 184–198. doi:10.1111/1462-2920.16285

Canovas, P. A., Hoehler, T., and Shock, E. L. (2017). Geochemical bioenergetics during low-temperature serpentinization: an example from the Samail ophiolite, Sultanate of Oman. *J. Geophys. Res. Biogeosciences* 122, 1821–1847. doi:10.1002/2017JG003825

Cardace, D., Hoehler, T., McCollom, T., Schrenk, M., Carnevale, D., Kubo, M., et al. (2013). Establishment of the Coast Range ophiolite microbial observatory (CROMO): drilling objectives and preliminary outcomes. *Sci. Drill.* 16, 45–55. doi:10.5194/sd-16-45-2013

Cardace, D., Meyer-Dombard, D. R., Woycheese, K. M., and Arcilla, C. A. (2015). Feasible metabolisms in high pH springs of the Philippines. *Front. Microbiol.* 6, 10. doi:10.3389/fmicb.2015.00010

Chavagnac, V., Monnin, C., Ceuleneer, G., Boulart, C., and Hoareau, G. (2013). Characterization of hyperalkaline fluids produced by low-temperature serpentinization of mantle peridotites in the Oman and Ligurian ophiolites. *Geochem. Geophys. Geosystems* 14, 2496–2522. doi:10.1002/ggge.20147

Chen, X., Ottosen, L. D. M., and Kofoed, M. V. W. (2019). How low can you go: methane production of Methanobacterium congolense at low CO2 concentrations. *Front. Bioeng. Biotechnol.* 7, 34. doi:10.3389/fbioe.2019.00034

Colman, D. R., Kraus, E. A., Thieringer, P. H., Rempfert, K., Templeton, A. S., Spear, J. R., et al. (2022). Deep-branching acetogens in serpentinized subsurface fluids of Oman. *Proc. Natl. Acad. Sci. U. S. A.* 119, e2206845119. doi:10.1073/pnas.2206845119

Colman, D. R., Poudel, S., Stamps, B. W., Boyd, E. S., and Spear, J. R. (2017). The deep, hot biosphere: Twenty-five years of retrospection. *Proc. Natl. Acad. Sci.* 114, 6895–6903. doi:10.1073/pnas.1701266114

Combaudon, V., Moretti, I., Kleine, B. I., and Stefánsson, A. (2022). Hydrogen emissions from hydrothermal fields in Iceland and comparison with the Mid-Atlantic Ridge. *Int. J. Hydrogen Energy* 47, 10217–10227. doi:10.1016/j.ijhydene.2022.01.101

Cook, M. C., Blank, J. G., Rietze, A., Suzuki, S., Nealson, K. H., and Morrill, P. L. (2021). A geochemical comparison of three terrestrial sites of serpentinization: the tablelands, the cedars, and aqua de Ney. *J. Geophys. Res. Biogeosciences* 126, e2021JG006316. doi:10.1029/2021JG006316

Coveney, R. M., Jr., Goebel, E. D., Zeller, E. J., Dreschhoff, G. A. M., and Angino, E. E. (1987). Serpentinization and the origin of hydrogen gas in Kansas. *AAPG Bull.* 71, 39–48. doi:10.1306/94886D3F-1704-11D7-8645000102C1865D

Deville, E., and Prinzhofer, A. (2016). The origin of N2-H2-CH4-rich natural gas seepages in ophiolitic context: a major and noble gases study of fluid seepages in New Caledonia. *Chem. Geol.* 440, 139–147. doi:10.1016/j.chemgeo.2016.06.011

Dewandel, B., Lachassagne, P., Boudier, F., Al-Hattali, S., Ladouche, B., Pinault, J.-L., et al. (2005). A conceptual hydrogeological model of ophiolite hard-rock aquifers in Oman based on a multiscale and a multidisciplinary approach. *Hydrogeol. J.* 13, 708–726. doi:10.1007/s10040-005-0449-2

Dunham, E. C., Dore, J. E., Skidmore, M. L., Roden, E. E., and Boyd, E. S. (2021). Lithogenic hydrogen supports microbial primary production in subglacial and proglacial environments. *Proc. Natl. Acad. Sci. U. S. A.* 118, e2007051117. doi:10.1073/pnas.2007051117

Ellison, E. T. (2024). Stimulated geological hydrogen production. Available at https://ericellison.shinyapps.io/gain_loss/ (Accessed January 4, 2024).

Ellison, E. T., Templeton, A. S., Zeigler, S. D., Mayhew, L. E., Kelemen, P. B., Matter, J. M., et al. (2021). Low-temperature hydrogen formation during aqueous alteration of serpentinized peridotite in the Samail ophiolite. *J. Geophys. Res. Solid Earth* 126, e2021JB021981. doi:10.1029/2021JB021981

Ely, T. D., Leong, J. M., Canovas, P. A., and Shock, E. L. (2023). Huge variation in H2 generation during seawater alteration of ultramafic rocks. *Geochem. Geophys. Geosystems* 24, e2022GC010658. doi:10.1029/2022GC010658

Escario, S., Godard, M., Gouze, P., and Leprovost, R. (2018). Experimental study of the effects of solute transport on reaction paths during incipient serpentinization. *Lithos* 323, 191–207. doi:10.1016/j.lithos.2018.09.020

Etiope, G., Samardžić, N., Grassa, F., Hrvatović, H., Miošić, N., and Skopljak, F. (2017). Methane and hydrogen in hyperalkaline groundwaters of the serpentinized Dinaride ophiolite belt, Bosnia and Herzegovina. *Appl. Geochem.* 84, 286–296. doi:10.1016/j.apgeochem.2017.07.006

Etiope, G., Schoell, M., and Hosgörmez, H. (2011). Abiotic methane flux from the Chimaera seep and Tekirova ophiolites (Turkey): understanding gas exhalation from low temperature serpentinization and implications for Mars. *Earth Planet. Sci. Lett.* 310, 96–104. doi:10.1016/j.epsl.2011.08.001

Fones, E. M., Colman, D. R., Kraus, E. A., Nothaft, D. B., Poudel, S., Rempfert, K. R., et al. (2019). Physiological adaptations to serpentinization in the Samail ophiolite, Oman. *ISME J.* 13, 1750–1762. doi:10.1038/s41396-019-0391-2

Fones, E. M., Colman, D. R., Kraus, E. A., Stepanauskas, R., Templeton, A. S., Spear, J. R., et al. (2021). Diversification of methanogens into hyperalkaline serpentinizing environments through adaptations to minimize oxidant limitation. *ISME J.* 15, 1121–1135. doi:10.1038/s41396-020-00838-1

Fones, E. M., Templeton, A. S., Mogk, D. W., and Boyd, E. S. (2022). Transformation of low-molecular-weight organic acids by microbial endoliths in subsurface mafic and ultramafic igneous rock. *Environ. Microbiol.* 24, 4137–4152. doi:10.1111/1462-2920.16041

Frost, B. R., and Beard, J. S. (2007). On silica activity and serpentinization. *J. Petrology* 48, 1351–1368. doi:10.1093/petrology/egm021

Frost, B. R., Evans, K. A., Swapp, S. M., Beard, J. S., and Mothersole, F. E. (2013). The process of serpentinization in dunite from New Caledonia. *Lithos* 178, 24–39. doi:10.1016/j.lithos.2013.02.002

Gaucher, E. C., Moretti, I., Pélissier, N., Burridge, G., and Gonthier, N. (2023). The place of natural hydrogen in the Energy Transition: a position paper. doi:10.5281/zenodo.8108239

Geymond, U., Briolet, T., Combaudon, V., Sissmann, O., Martinez, I., Duttine, M., et al. (2023). Reassessing the role of magnetite during natural hydrogen generation. *Front. Earth Sci.* 11. doi:10.3389/feart.2023.1169356

Glombitza, C., Putman, L. I., Rempfert, K. R., Kubo, M. D., Schrenk, M. O., Templeton, A. S., et al. (2021). Active microbial sulfate reduction in fluids of serpentinizing peridotites of the continental subsurface. *Commun. Earth Environ.* 2, 84. doi:10.1038/s43247-021-00157-z

Godard, M., Jousselin, D., and Bodinier, J. L. (2000). Relationships between geochemistry and structure beneath a palaeo-spreading centre: a study of the mantle section in the Oman ophiolite. *Earth Planet. Sci. Lett.* 180 (1-2), 133–148. doi:10.1016/s0012-821x(00)00149-7

Godard, M., Luquot, L., Andreani, M., and Gouze, P. (2013). Incipient hydration of mantle lithosphere at ridges: a reactive-percolation experiment. *Earth Planet. Sci. Lett.* 371-372, 92–102. doi:10.1016/j.epsl.2013.03.052

Greening, C., Biswas, A., Carere, C. R., Jackson, C. J., Taylor, M. C., Stott, M. B., et al. (2016). Genomic and metagenomic surveys of hydrogenase distribution indicate H2 is a widely utilised energy source for microbial growth and survival. *ISME J.* 10, 761–777. doi:10.1038/ismej.2015.153

Grozeva, N. G., Klein, F., Seewald, J. S., and Sylva, S. P. (2017). Experimental study of carbonate formation in oceanic peridotite. *Geochimica Cosmochimica Acta* 199, 264–286. doi:10.1016/j.gca.2016.10.052

Hanghoj, K., Kelemen, P. B., Hassler, D., and Godard, M. (2010). Composition and genesis of depleted mantle peridotites from the Wadi Tayin massif, Oman ophiolite; Major and trace element geochemistry, and Os isotope and PGE systematics. *J. Petrology* 51, 201–227. doi:10.1093/petrology/egp077

Hellevang, H., Huang, S., and Thorseth, I. H. (2011). The potential for low-temperature abiotic hydrogen generation and a hydrogen-driven deep biosphere. *Astrobiology* 11, 711–724. doi:10.1089/ast.2010.0559

Hoehler, T. M., Mankel, D. J., Girguis, P. R., McCollom, T. M., Kiang, N. Y., and Jørgensen, B. B. (2023). The metabolic rate of the biosphere and its components. *Proc. Natl. Acad. Sci. U. S. A.* 120, e2303764120. doi:10.1073/pnas.2303764120

Homma, S., Ogata, S., Koga, J., and Matsumoto, S. (2005). Gas–solid reaction model for a shrinking spherical particle with unreacted shrinking core. *Chem. Eng. Sci.* 60, 4971–4980. doi:10.1016/j.ces.2005.03.057

Hong, G., Till, J. L., Greve, A., and Lee, S.-M. (2022). New rock magnetic analysis of ultramafic cores from the Oman drilling project and its implications for alteration of lower crust and upper mantle. *J. Geophys. Res. Solid Earth* 127, e2022JB024379. doi:10.1029/2022JB024379

Hosgormez, H., Etiope, G., and Yalçin, M. N. (2008). New evidence for a mixed inorganic and organic origin of the Olympic Chimaera fire (Turkey): a large onshore seepage of abiogenic gas. *Geofluids* 8, 263–273. doi:10.1111/j.1468-8123.2008.00226.x

Howells, A. E. G., Leong, J. A. M., Ely, T., Santana, M., Robinson, K., Esquivel-Elizondo, S., et al. (2022). Energetically informed niche models of hydrogenotrophs detected in sediments of serpentinized fluids of the Samail ophiolite of Oman. *J. Geophys. Res. Biogeosciences* 127, e2021JG006317. doi:10.1029/2021JG006317

Iyer, K., Jamtveit, B., Mathiesen, J., Malthe-Sørenssen, A., and Feder, J. (2008). Reaction-assisted hierarchical fracturing during serpentinization. *Earth Planet. Sci. Lett.* 267, 503–516. doi:10.1016/j.epsl.2007.11.060

Jamtveit, B., Malthe-Sørenssen, A., and Kostenko, O. (2008). Reaction enhanced permeability during retrogressive metamorphism. *Earth Planet. Sci. Lett.* 267, 620–627. doi:10.1016/j.epsl.2007.12.016

Kato, S., and Ohkuma, M. (2021). A single bacterium capable of oxidation and reduction of iron at circumneutral pH. *Microbiol. Spectr.* 9, e0016121. doi:10.1128/spectrum.00161-21

Kelemen, P. B., and Hirth, G. (2012). Reaction-driven cracking during retrograde metamorphism: olivine hydration and carbonation. *Earth Planet. Sci. Lett.* 345–348, 81–89. doi:10.1016/j.epsl.2012.06.018

Kelemen, P. B., Leong, J. A., Carlos de Obeso, J., Matter, J. M., Ellison, E. T., Templeton, A., et al. (2021). Initial results from the Oman Drilling Project Multi-Borehole Observatory: petrogenesis and ongoing alteration of mantle peridotite in the weathering horizon. *J. Geophys. Res. Solid Earth* 126, e2021JB022729. doi:10.1029/2021JB022729

Kelemen, P. B., and Matter, J. (2008). *In situ* carbonation of peridotite for CO_2 storage. *Proc. Natl. Acad. Sci.* 105, 17295–17300. doi:10.1073/pnas.0805794105

Kelemen, P. B., Matter, J. M., Teagle, D. A. H., and Coggon, J. A. (2020). Proceedings of the Oman drilling project: scientific drilling in the Samail ophiolite, sultanate of Oman. *Proc. Int. Ocean Discov. Program*. doi:10.14379/OmanDP.proc.2020

Klein, F., and Bach, W. (2009). Fe–Ni–Co–O–S phase relations in peridotite–seawater interactions. *J. Petrology* 50, 37–59. doi:10.1093/petrology/egn071

Klein, F., Bach, W., Humphris, S. E., Kahl, W.-A., Jöns, N., Moskowitz, B., et al. (2014). Magnetite in seafloor serpentinite—some like it hot. *Geology* 42, 135–138. doi:10.1130/G35068.1

Klein, F., Bach, W., Jöns, N., McCollom, T., Moskowitz, B., and Berquó, T. (2009). Iron partitioning and hydrogen generation during serpentinization of abyssal peridotites from 15°N on the Mid-Atlantic Ridge. *Geochimica Cosmochimica Acta* 73, 6868–6893. doi:10.1016/j.gca.2009.08.021

Klein, F., Bach, W., and McCollom, T. M. (2013). Compositional controls on hydrogen generation during serpentinization of ultramafic rocks. *Lithos* 178, 55–69. doi:10.1016/j.lithos.2013.03.008

Klein, F., Tarnas, J. D., and Bach, W. (2020). Abiotic sources of molecular hydrogen on Earth. *Elements* 16 (1), 19–24. doi:10.2138/gselements.16.1.19

Kraus, E. A., Nothaft, D. B., Stamps, B. W., Rempfert, K. R., Ellison, E. T., Matter, J. M., et al. (2021). Molecular evidence for an active microbial methane cycle in subsurface serpentinite-hosted groundwaters in the Samail ophiolite, Oman. *Appl. Environ. Microbiol.* 87. doi:10.1128/AEM.02068-20

Kuzma, S., Saccoccia, L., and Chertock, M. (2023). 25 countries, housing one-quarter of the population, face extremely high water stress. Available at https://www.wri.org/insights/highest-water-stressed-countries (Accessed January 4, 2024).

Lafay, R., Montes-Hernandez, G., Janots, E., Chiriac, R., Findling, N., and Toche, F. (2012). Mineral replacement rate of olivine by chrysotile and brucite under high alkaline conditions. *J. Cryst. Growth* 347, 62–72. doi:10.1016/j.jcrysgro.2012.02.040

Lamadrid, H. M., Zajacz, Z., Klein, F., and Bodnar, R. J. (2021). Synthetic fluid inclusions XXIII. Effect of temperature and fluid composition on rates of serpentinization of olivine. *Geochimica Cosmochimica Acta* 292, 285–308. doi:10.1016/j.gca.2020.08.009

Lefeuvre, N., Truche, L., Donzé, F., Ducoux, M., Barré, G., Fakoury, R., et al. (2021). Native H_2 exploration in the western pyrenean foothills. *Geochem. Geophys. Geosystems* 22. doi:10.1029/2021GC009917

Leong, J. A., Nielsen, M., McQueen, N., Karolytė, R., Hillegonds, D. J., Ballentine, C., et al. (2023). H_2 and CH_4 outgassing rates in the Samail ophiolite, Oman: implications for low-temperature, continental serpentinization rates. *Geochimica Cosmochimica Acta* 347, 1–15. doi:10.1016/j.gca.2023.02.008

Leong, J. A. M., Ely, T., and Shock, E. L. (2021a). Decreasing extents of Archean serpentinization contributed to the rise of an oxidized atmosphere. *Nat. Commun.* 12, 7341. doi:10.1038/s41467-021-27589-7

Leong, J. a. M., Howells, A. E., Robinson, K. J., Cox, A., Debes, R. V., Fecteau, K., et al. (2021b). Theoretical predictions versus environmental observations on serpentinization fluids: lessons from the Samail ophiolite in Oman. *J. Geophys. Res. Solid Earth* 126, e2020JB020756. doi:10.1029/2020JB020756

Leong, J. A. M., and Shock, E. L. (2020). Thermodynamic constraints on the geochemistry of low-temperature, continental, serpentinization-generated fluids. *Am. J. Sci.* 320, 185–235. doi:10.2475/03.2020.01

Lie, T. J., Costa, K. C., Lupa, B., Korpole, S., Whitman, W. B., and Leigh, J. A. (2012). Essential anaplerotic role for the energy-converting hydrogenase Eha in hydrogenotrophic methanogenesis. *Proc. Natl. Acad. Sci. U. S. A.* 109, 15473–15478. doi:10.1073/pnas.1208779109

Lods, G., Roubinet, D., Matter, J. M., Leprovost, R., and Gouze, P. (2020). Groundwater flow characterization of an ophiolitic hard-rock aquifer from cross-borehole multi-level hydraulic experiments. *J. Hydrology* 589, 125152. doi:10.1016/j.jhydrol.2020.125152

Lollar, B. S., Onstott, T. C., Lacrampe-Couloume, G., and Ballentine, C. J. (2014). The contribution of the Precambrian continental lithosphere to global H2 production. *Nature* 516 (7531), 379–382. doi:10.1038/nature14017

Malvoisin, B., Brunet, F., Carlut, J., Rouméjon, S., and Cannat, M. (2012). Serpentinization of oceanic peridotites: 2. Kinetics and processes of San Carlos olivine hydrothermal alteration. *J. Geophys. Res. Solid Earth* 117. doi:10.1029/2011JB008842

Manatschal, G., and Müntener, O. (2009). A type sequence across an ancient magma-poor ocean–continent transition: the example of the western Alpine Tethys ophiolites. *Tectonophysics* 473, 4–19. doi:10.1016/j.tecto.2008.07.021

Martin, B., and Fyfe, W. S. (1970). Some experimental and theoretical observations on the kinetics of hydration reactions with particular reference to serpentinization. *Chem. Geol.* 6, 185–202. doi:10.1016/0009-2541(70)90018-5

Martin, W. F. (2012). Hydrogen, metals, bifurcating electrons, and proton gradients: the early evolution of biological energy conservation. *FEBS Lett.* 586, 485–493. doi:10.1016/j.febslet.2011.09.031

Mayhew, L. E., and Ellison, E. T. (2020). A synthesis and meta-analysis of the Fe chemistry of serpentinites and serpentine minerals. *Philosophical Trans. R. Soc. A Math. Phys. Eng. Sci.* 378, 20180420. doi:10.1098/rsta.2018.0420

Mayhew, L. E., Ellison, E. T., McCollom, T. M., Trainor, T. P., and Templeton, A. S. (2013). Hydrogen generation from low-temperature water–rock reactions. *Nat. Geosci.* 6, 478–484. doi:10.1038/ngeo1825

Mayhew, L. E., Ellison, E. T., Miller, H. M., Kelemen, P. B., and Templeton, A. S. (2018). Iron transformations during low temperature alteration of variably serpentinized rocks from the Samail ophiolite, Oman. *Geochimica Cosmochimica Acta* 222, 704–728. doi:10.1016/j.gca.2017.11.023

McCollom, T. M., and Bach, W. (2009). Thermodynamic constraints on hydrogen generation during serpentinization of ultramafic rocks. *Geochimica Cosmochimica Acta* 73, 856–875. doi:10.1016/j.gca.2008.10.032

McCollom, T. M., Klein, F., Moskowitz, B., Berquó, T. S., Bach, W., and Templeton, A. S. (2020a). Hydrogen generation and iron partitioning during experimental serpentinization of an olivine–pyroxene mixture. *Geochimica Cosmochimica Acta* 282, 55–75. doi:10.1016/j.gca.2020.05.016

McCollom, T. M., Klein, F., Robbins, M., Moskowitz, B., Berquó, T. S., Jöns, N., et al. (2016). Temperature trends for reaction rates, hydrogen generation, and partitioning of iron during experimental serpentinization of olivine. *Geochimica Cosmochimica Acta* 181, 175–200. doi:10.1016/j.gca.2016.03.002

McCollom, T. M., Klein, F., Solheid, P., and Moskowitz, B. (2020b). The effect of pH on rates of reaction and hydrogen generation during serpentinization. *Philosophical Trans. R. Soc. A Math. Phys. Eng. Sci.* 378, 20180428. doi:10.1098/rsta.2018.0428

McCollom, T. M., and Shock, E. L. (1997). Geochemical constraints on chemolithoautotrophic metabolism by microorganisms in seafloor hydrothermal systems. *Geochimica Cosmochimica Acta* 61, 4375–4391. doi:10.1016/s0016-7037(97)00241-x

Merdith, A. S., del Real, P. G., Daniel, I., Andreani, M., Wright, N. M., and Coltice, N. (2020). Pulsated global hydrogen and methane flux at mid-ocean ridges driven by Pangea breakup. *Geochem. Geophys. Geosystems* 21 (4), e2019GC008869. doi:10.1029/2019gc008869

Miller, H. M., Matter, J. M., Kelemen, P. B., Ellison, E. T., Conrad, M. E., Fierer, N., et al. (2016). Modern water/rock reactions in Oman hyperalkaline peridotite aquifers and implications for microbial habitability. *Geochimica Cosmochimica Acta* 179, 217–241. doi:10.1016/j.gca.2016.01.033

Miller, H. M., Mayhew, L. E., Ellison, E. T., Kelemen, P. B., Kubo, M., and Templeton, A. S. (2017). Low temperature hydrogen production during experimental hydration of partially-serpentinized dunite. *Geochimica Cosmochimica Acta* 209, 161–183. doi:10.1016/j.gca.2017.04.022

Monnier, C., Girardeau, J., Le Mée, L., and Polvé, M. (2006). Along-ridge petrological segmentation of the mantle in the Oman ophiolite. *Geochem. Geophys. Geochem. Geophys. Geosystems* 7. doi:10.1029/2006GC001320

Monnin, C., Chavagnac, V., Boulart, C., Ménez, B., Gérard, M., Gérard, E., et al. (2014). Fluid chemistry of the low temperature hyperalkaline hydrothermal system of Prony Bay (New Caledonia). *Biogeosciences* 11, 5687–5706. doi:10.5194/bg-11-5687-2014

Monnin, C., Quéméneur, M., Price, R., Jeanpert, J., Maurizot, P., Boulart, C., et al. (2021). The chemistry of hyperalkaline springs in serpentinizing environments: 1. The composition of free gases in New Caledonia compared to other springs worldwide. *J. Geophys. Res. Biogeosciences* 126, e2021JG006243. doi:10.1029/2021JG006243

Moretti, I., Geymond, U., Pasquet, G., Aimar, L., and Rabaute, A. (2022). Natural hydrogen emanations in Namibia: field acquisition and vegetation indexes from multispectral satellite image analysis. *Int. J. Hydrogen Energy* 47, 35588–35607. doi:10.1016/j.ijhydene.2022.08.135

Moretti, I., Prinzhofer, A., Françolin, J., Pacheco, C., Rosanne, M., Rupin, F., et al. (2021). Long-term monitoring of natural hydrogen superficial emissions in a brazilian cratonic environment. Sporadic large pulses versus daily periodic emissions. *Int. J. Hydrogen Energy* 46, 3615–3628. doi:10.1016/j.ijhydene.2020.11.026

Morrill, P. L., Kuenen, J. G., Johnson, O. J., Suzuki, S., Rietze, A., Sessions, A. L., et al. (2013). Geochemistry and geobiology of a present-day serpentinization site in California: the Cedars. *Geochimica Cosmochimica Acta* 109, 222–240. doi:10.1016/j.gca.2013.01.043

Munro-Ehrlich, M., Nothaft, D. B., Fones, E. M., Matter, J. M., Templeton, A. S., and Boyd, E. S. (2023). Parapatric speciation of Meiothermus in serpentinite-hosted aquifers in Oman. *Front. Microbiol.* 14, 1138656. doi:10.3389/fmicb.2023.1138656

Neal, C., and Stanger, G. (1983). Hydrogen generation from mantle source rocks in Oman. *Earth Planet. Sci. Lett.* 66, 315–320. doi:10.1016/0012-821X(83)90144-9

Nealson, K. H., Inagaki, F., and Takai, K. (2005). Hydrogen-driven subsurface lithoautotrophic microbial ecosystems (SLiMEs): do they exist and why should we care? *Trends Microbiol.* 13, 405–410. doi:10.1016/j.tim.2005.07.010

Nesbitt, H. W., and Bricker, O. P. (1978). Low temperature alteration processes affecting ultramafic bodies. *Geochimica Cosmochimica Acta* 42, 403–409. doi:10.1016/0016-7037(78)90271-5

Net Zero (2022). Oman Ministry of energy and minerals. Available at https://www.ea.gov.om/media/aaslyc3l/oman-net-zero-report-2022_screen.pdf.

Nicolas, A., Boudier, F., Ildefonse, B., and Ball, E. (2000). Accretion of Oman and United Arab Emirates ophiolite – discussion of a new structural map. *Mar. Geophys. Res.* 21, 147–180. doi:10.1023/A:1026769727917

Ninkabou, D., Agard, P., Nielsen, C., Smit, J., Gorini, C., Rodriguez, M., et al. (2021). Structure of the offshore obducted Oman margin: emplacement of semail ophiolite and role of tectonic inheritance. *J. Geophys. Res. Solid Earth* 126, 2020JB020187. doi:10.1029/2020JB020187

Noël, J., Godard, M., Oliot, E., Martinez, I., Williams, M., Boudier, F., et al. (2018). Evidence of polygenetic carbon trapping in the Oman Ophiolite: petro-structural, geochemical, and carbon and oxygen isotope study of the Wadi Dima harzburgite-hosted carbonates (Wadi Tayin massif, Sultanate of Oman). *Lithos* 323, 218–237. doi:10.1016/j.lithos.2018.08.020

Nothaft, D. B. (2020). Bubble strip aqueous gas sampling. *Protoc. Io*. doi:10.17504/protocols.io.bkb9ksr6

Nothaft, D. B., Templeton, A. S., Boyd, E., Matter, J., Stute, M., and Vankeuren, P. (2021a). Aqueous geochemical and microbial variation across discrete depth intervals in a peridotite aquifer assessed using a packer system in the Samail Ophiolite. *Oman. Earth Space Sci. Open Arch*. 34. doi:10.1002/essoar.10506402.2

Nothaft, D. B., Templeton, A. S., Boyd, E. S., Matter, J. M., Stute, M., Paukert Vankeuren, A. N., et al. (2021b). Aqueous geochemical and microbial variation across discrete depth intervals in a peridotite aquifer assessed using a packer system in the Samail ophiolite, Oman. *J. Geophys. Res. Biogeosciences* 126, 49. doi:10.1029/2021JG006319

Oelkers, E. H., Declercq, J., Saldi, G. D., Gislason, S. R., and Schott, J. (2018). Olivine dissolution rates: a critical review. *Chem. Geol.* 500, 1–19. doi:10.1016/j.chemgeo.2018.10.008

Ogasawara, Y., Okamoto, A., Hirano, N., and Tsuchiya, N. (2013). Coupled reactions and silica diffusion during serpentinization. *Geochimica Cosmochimica Acta* 119, 212–230. doi:10.1016/j.gca.2013.06.001

Okamoto, A., Ogasawara, Y., Ogawa, Y., and Tsuchiya, N. (2011). Progress of hydration reactions in olivine–H2O and orthopyroxenite–H2O systems at 250 °C and vapor-saturated pressure. *Chem. Geol.* 289, 245–255. doi:10.1016/j.chemgeo.2011.08.007

Oman Vision (2023). Oman vision 2040 implementation follow-up unit available at. https://www.oman2040.om/Oman2040Report (Accessed January 4, 2024).

Osselin, F., Soulaine, C., Fauguerolles, C., Gaucher, E. C., Scaillet, B., and Pichavant, M. (2022). Orange hydrogen is the new green. *Nat. Geosci.* 15, 765–769. doi:10.1038/s41561-022-01043-9

Oufi, O., Cannat, M., and Horen, H. (2002). Magnetic properties of variably serpentinized abyssal peridotites. *J. Geophys. Res. Solid Earth* 107. doi:10.1029/2001JB000549

Oyanagi, R., Okamoto, A., and Tsuchiya, N. (2020). Silica controls on hydration kinetics during serpentinization of olivine: Insights from hydrothermal experiments and a reactive transport model. *Geochim Cosmochim Acta* 270, 21–42. doi:10.1016/j.gca.2019.11.017

Pasquet, G., Houssein Hassan, R., Sissmann, O., Varet, J., and Moretti, I. (2021). An attempt to study natural H2 resources across an oceanic ridge penetrating a continent: the asal–ghoubbet rift (republic of Djibouti). *Geosciences* 12, 16. doi:10.3390/geosciences12010016

Paukert, A. N., Matter, J. M., Kelemen, P. B., Shock, E. L., and Havig, J. R. (2012). Reaction path modeling of enhanced *in situ* CO_2 mineralization for carbon sequestration in the peridotite of the Samail Ophiolite, Sultanate of Oman. *Chem. Geol.* 330–331, 86–100. doi:10.1016/j.chemgeo.2012.08.013

Paukert Vankeuren, A. N., Matter, J. M., Stute, M., and Kelemen, P. B. (2019). Multitracer determination of apparent groundwater ages in peridotite aquifers within the Samail ophiolite, Sultanate of Oman. *Earth Planet. Sci. Lett.* 516, 37–48. doi:10.1016/j.epsl.2019.03.007

Peters, J. W., Schut, G. J., Boyd, E. S., Mulder, D. W., Shepard, E. M., Broderick, J. B., et al. (2015). [FeFe]- and [NiFe]-hydrogenase diversity, mechanism, and maturation. *Biochimica Biophysica Acta (BBA) - Mol. Cell Res.* 1853, 1350–1369. doi:10.1016/j.bbamcr.2014.11.021

Peuble, S., Godard, M., Luquot, L., Andreani, M., Martinez, I., and Gouze, P. (2015). CO_2 geological storage in olivine rich basaltic aquifers: new insights from reactive-percolation experiments. *Appl. Geochem.* 52, 174–190. doi:10.1016/j.apgeochem.2014.11.024

Plümper, O., Beinlich, A., Bach, W., Janots, E., and Austrheim, H. (2014). Garnets within geode-like serpentinite veins: implications for element transport, hydrogen production and life-supporting environment formation. *Geochimica Cosmochimica Acta* 141, 454–471. doi:10.1016/j.gca.2014.07.002

Rempfert, K. R., Miller, H. M., Bompard, N., Nothaft, D. B., Matter, J. M., Kelemen, P. B., et al. (2017). Geological and geochemical controls on subsurface microbial life in the Samail ophiolite, Oman. *Front. Microbiol.* 8, 56. doi:10.3389/fmicb.2017.00056

Rempfert, K. R., Nothaft, D. B., Kraus, E. A., Asamoto, C. K., Evans, R. D., Spear, J. R., et al. (2023). Subsurface biogeochemical cycling of nitrogen in the actively serpentinizing Samail Ophiolite, Oman. *Front. Microbiol.* 14, 1139633. doi:10.3389/fmicb.2023.1139633

Rudge, J. F., Kelemen, P. B., and Spiegelman, M. (2010). A simple model of reaction-induced cracking applied to serpentinization and carbonation of peridotite. *Earth Planet. Sci. Lett.* 291, 215–227. doi:10.1016/j.epsl.2010.01.016

Russo, V., Grénman, H., Cogliano, T., Tesser, R., and Salmi, T. (2020). Advanced shrinking particle model for fluid-reactive solid systems. *Front. Chem. Eng.* Sec. Chemical Reaction Engineering 2. doi:10.3389/fceng.2020.577505

Sabuda, M. C., Putman, L. I., Hoehler, T. M., Kubo, M. D., Brazelton, W. J., Cardace, D., et al. (2021). Biogeochemical gradients in a serpentinization-influenced aquifer: implications for gas exchange between the subsurface and atmosphere. *J. Geophys. Res.* 126 (8), e2020JG006209.

Sano, Y., Urabe, A., Wakita, H., Chiba, H., and Sakai, H. (1985). Chemical and isotopic compositions of gases in geothermal fluids in Iceland. *Geochem. J.* 19, 135–148. doi:10.2343/geochemj.19.135

Schrenk, M. O., Brazelton, W. J., and Lang, S. Q. (2013). Serpentinization, carbon, and deep life. *Rev. Mineral. Geochem.* 75 (1), 575–606.

Scicchitano, M. R., Spicuzza, M. J., Ellison, E. T., Tuschel, D., Templeton, A. S., and Valley, J. W. (2020). *In situ* oxygen isotope determination in serpentine minerals by SIMS: addressing matrix effects and providing new insights on serpentinisation at Hole BA1B (Samail ophiolite, Oman). *Geostand. Geoanalytical Res.* 45, 161–187. doi:10.1111/ggr.12359

Seyfried, W. E., Foustoukos, D. I., and Fu, Q. (2007). Redox evolution and mass transfer during serpentinization: an experimental and theoretical study at 200°C, 500bar with implications for ultramafic-hosted hydrothermal systems at Mid-Ocean Ridges. *Geochimica Cosmochimica Acta* 71, 3872–3886. doi:10.1016/j.gca.2007.05.015

Sherwood Lollar, B., Ballentine, C. J., and Onions, R. K. (1997). The fate of mantle-derived carbon in a continental sedimentary basin: integration of relationships and stable isotope signatures. *Geochimica Cosmochimica Acta* 61, 2295–2307. doi:10.1016/S0016-7037(97)00083-5

Sherwood Lollar, B., Frape, S. K., Weise, S. M., Fritz, P., Macko, S. A., and Welhan, J. A. (1993). Abiogenic methanogenesis in crystalline rocks. *Geochimica Cosmochimica Acta* 57, 5087–5097. doi:10.1016/0016-7037(93)90610-9

Sleep, N. H., Meibom, A., Fridriksson, T., Coleman, R. G., and Bird, D. K. (2004). H_2-rich fluids from serpentinization: geochemical and biotic implications. *Proc. Natl. Acad. Sci. U. S. A.* 101, 12818–12823. doi:10.1073/pnas.0405289101

Sohn, R. A., and Matter, J. M. (2023). The response of borehole water levels in an ophiolitic, peridotite aquifer to atmospheric, solid Earth, and ocean tides. *J. Hydrology X* 21, 100163. doi:10.1016/j.hydroa.2023.100163

Søndergaard, D., Pedersen, C. N. S., and Greening, C. (2016). HydDB: a web tool for hydrogenase classification and analysis. *Sci. Rep.* 6, 34212. doi:10.1038/srep34212

Song, H., Ou, X., Han, B., Deng, H., Zhang, W., Tian, C., et al. (2021). An overlooked natural hydrogen evolution pathway: Ni^{2+} boosting water reduction by $Fe(OH)_2$ oxidation during low-temperature serpentinization. *Angew. Chem. Int. Ed.* 60, 24054–24058. doi:10.1002/anie.202110653

Steefel, C. I., DePaolo, D. J., and Lichtner, P. C. (2005). Reactive transport modeling: an essential tool and a new research approach for the Earth sciences. *Earth Planet. Sci. Lett.* 240 (3-4), 539–558. doi:10.1016/j.epsl.2005.09.017

Strohm, T. O., Griffin, B., Zumft, W. G., and Schink, B. (2007). Growth yields in bacterial denitrification and nitrate ammonification. *Appl. Environ. Microbiol.* 73, 1420–1424. doi:10.1128/AEM.02508-06

Suzuki, S., Ishii, S., Wu, A., Cheung, A., Tenney, A., Wanger, G., et al. (2013). Microbial diversity in the Cedars, an ultrabasic, ultrareducing, and low salinity serpentinizing ecosystem. *Proc. Natl. Acad. Sci.* 110, 15336–15341. doi:10.1073/pnas.1302426110

Szponar, N., Brazelton, W. J., Schrenk, M. O., Bower, D. M., Steele, A., and Morrill, P. L. (2013). Geochemistry of a continental site of serpentinization, the tablelands ophiolite, gros morne national park: a mars analogue. *Icarus* 224, 286–296. doi:10.1016/j.icarus.2012.07.004

Templeton, A. S., and Caro, T. A. (2023). The rock-hosted biosphere. *Annu. Rev. Earth Planet. Sci.* 51, 493–519. doi:10.1146/annurev-earth-031920-081957

Templeton, A. S., and Ellison, E. T. (2020). Formation and loss of metastable brucite: does Fe(II)-bearing brucite support microbial activity in serpentinizing ecosystems? *Philosophical Trans. R. Soc. A Math. Phys. Eng. Sci.* 378, 20180423. doi:10.1098/rsta.2018.0423

Templeton, A. S., Ellison, E. T., Glombitza, C., Morono, Y., Rempfert, K. R., Hoehler, T. M., et al. (2021). Accessing the subsurface biosphere within rocks undergoing active low-temperature serpentinization in the Samail ophiolite (Oman drilling project). *J. Geophys. Res. Biogeosciences* 126, e2021JG006315. doi:10.1029/2021JG006315

Thieringer, P. H., Boyd, E. S., Templeton, A. S., and Spear, J. R. (2023). Metapangenomic investigation provides insight into niche differentiation of methanogenic populations from the subsurface serpentinizing environment, Samail Ophiolite, Oman. *Front. Microbiol.* 14, 1205558. doi:10.3389/fmicb.2023.1205558

Toft, P. B., Arkani-Hamed, J., and Haggerty, S. E. (1990). The effects of serpentinization on density and magnetic susceptibility: a petrophysical model. *Phys. Earth Planet. Interiors* 65, 137–157. doi:10.1016/0031-9201(90)90082-9

Truche, L., Joubert, G., Dargent, M., Martz, P., Cathelineau, M., Rigaudier, T., et al. (2018). Clay minerals trap hydrogen in the Earth's crust: evidence from the Cigar Lake uranium deposit, Athabasca. *Earth Planet. Sci. Lett.* 493, 186–197. doi:10.1016/j.epsl.2018.04.038

Tutolo, B. M., Luhmann, A. J., Tosca, N. J., and Seyfried, W. E. (2018). Serpentinization as a reactive transport process: the brucite silicification reaction. *Earth Planet. Sci. Lett.* 484, 385–395. doi:10.1016/j.epsl.2017.12.029

Tutolo, B. M., Seyfried, W. E., and Tosca, N. J. (2020). A seawater throttle on H_2 production in Precambrian serpentinizing systems. *Proc. Natl. Acad. Sci.* 117, 14756–14763. doi:10.1073/pnas.1921042117

Vacquand, C. (2011). Genesis and mobility of natural hydrogen: energy source or storable energy carrier? Available at https://inis.iaea.org/search/search.aspx?orig_q=RN:44098391 (Accessed December 27, 2023).

Vacquand, C., Deville, E., Beaumont, V., Guyot, F., Sissmann, O., Pillot, D., et al. (2018). Reduced gas seepages in ophiolitic complexes: evidences for multiple origins of the H_2-CH_4-N_2 gas mixtures. *Geochimica Cosmochimica Acta* 223, 437–461. doi:10.1016/j.gca.2017.12.018

Vignais, P. M., and Billoud, B. (2007). Occurrence, classification, and biological function of Hydrogenases: an overview. *Chem. Rev.* 107, 4206–4272. doi:10.1021/cr050196r

Vignais, P. M., Billoud, B., and Meyer, J. (2001). Classification and phylogeny of hydrogenases. *FEMS Microbiol. Rev.* 25, 455–501. doi:10.1111/j.1574-6976.2001.tb00587.x

Warr, O., Giunta, T., Ballentine, C. J., and Sherwood Lollar, B. (2019). Mechanisms and rates of 4He, 40Ar, and H2 production and accumulation in fracture fluids in Precambrian Shield environments. *Chem. Geol.* 530, 119322. doi:10.1016/j.chemgeo.2019.119322

Wegner, W. W., and Ernst, W. G. (1983). Experimentally determined hydration and dehydration reaction rates in the system MgO-SiO_2-H_2O. *Am. J. Sci.* 283, 151–180.

Zgonnik, V. (2020). The occurrence and geoscience of natural hydrogen: a comprehensive review. *Earth-Science Rev.* 203, 103140. doi:10.1016/j.earscirev.2020.103140

Zgonnik, V., Beaumont, V., Larin, N., Pillot, D., and Deville, E. (2019). Diffused flow of molecular hydrogen through the Western Hajar mountains, Northern Oman. *Arab. J. Geosci.* 12, 71. doi:10.1007/s12517-019-4242-2